



## **Seasonal variability, sources, and parameterization of ice-nucleating particles in the Rocky Mountain region**

**Ruichen Zhou, Russell Perkins, Drew Juergensen, Kevin Barry, Kelton Ayars, Oren Dutton,  
5 Paul DeMott, Sonia Kreidenweis**

Department of Atmospheric Science, Colorado State University, Fort Collins, Colorado 80523,  
USA

Corresponding author: Russell Perkins ([rperkins@colostate.edu](mailto:rperkins@colostate.edu))



## 15 Abstract

Atmospheric ice-nucleating particles (INPs) significantly influence cloud microphysics and aerosol-cloud interactions. Given that mountainous regions are vital to water resources, understanding of INPs in these areas is important for predicting impacts on regional clouds and precipitation. In this study, we conducted comprehensive measurements of immersion-freezing  
20 INPs at Mt. Crested Butte in the Rocky Mountains from September 2021 to June 2023 as part of the Surface Atmosphere Integrated Field Laboratory (SAIL) campaign. The average number concentration of INPs active at  $-20\text{ }^{\circ}\text{C}$  was  $2\text{ L}^{-1}$ , with distinct seasonal variation characterized by high summer concentrations and low winter concentrations. INP concentrations were correlated with a coarse dust aerosol type, which dominates  $\text{PM}_{10}$  in this region. Converting INP  
25 concentrations to IN active surface site densities ( $n_s$ ) led to reduction in variability, further supporting a relationship between coarse dust and INPs. Reduction of INP concentrations following treatment with  $\text{H}_2\text{O}_2$  indicated substantial contributions from organic INPs across all activation temperatures, suggesting that organic-containing soil dust dominates the INPs in this region. Heat-labile INPs, likely biological in origin, were identified as dominant at  $> -15\text{ }^{\circ}\text{C}$   
30 through heat treatment of samples and showed significantly lower contributions in winter. Parameterizations based on  $n_s$  for the INPs observed in this mountainous region were developed, which effectively reproduced measured INPs concentrations, particularly when accounting for seasonal differences. This study provides the first long-term, comprehensive characterization of INPs for the Upper Colorado River Basin region and offers a parameterization potentially useful  
35 for predicting INPs in other remote continental regions.



## 1. Introduction

Atmospheric aerosols play critical roles in forming clouds, and inadequate understanding of aerosol-cloud interactions presents one of the largest uncertainties in predicting global climate (IPCC, 2022; Seinfeld et al., 2016). The subset of aerosol particles that serves as ice-nucleating particles (INPs) can trigger heterogeneous freezing of cloud water droplets, allowing them to freeze above the homogeneous freezing temperature (approximately  $-38^{\circ}\text{C}$ ) (Hoose and Möhler, 2012). Among the mechanisms of heterogeneous freezing, this immersion freezing process is considered the most important process for mixed-phase clouds, which are common at midlatitudes in all seasons (Kanji et al., 2017; De Boer et al., 2011). These INPs are responsible for a significant proportion of initial cloud ice phase formation, thus impacting the Earth's radiative balance and precipitation (Lohmann and Feichter, 2005; Kanji et al., 2017; Burrows et al., 2022). Although INPs are increasingly a focus of study, the sources and abundances of INPs are not well characterized for many regions.

Various aerosol sources have been found to contribute to INPs, including natural and anthropogenic sources (Kanji et al., 2017). Atmospheric mineral dust particles are considered a dominant contributor of INPs throughout much of the troposphere, especially at colder temperatures (Murray et al., 2012; Hoose and Möhler, 2012). Mineral dust presents efficient ice nucleating ability at temperatures lower than  $-15^{\circ}\text{C}$  (Atkinson et al., 2013; Kiselev et al., 2017). Mineral INPs are inorganic components that are lofted from rock or soil and can undergo long range transport to remote areas (Knippertz and Stuut, 2014). In contrast, soil dusts from agricultural or grazed fields (arable soils) were suggested to contribute 25% of the global dust burden (Ginoux et al., 2012), and were found to initiate ice nucleation at temperatures as high as  $-6^{\circ}\text{C}$  (Garcia et al., 2012; O'Sullivan et al., 2014). Organics in arable soil dust are suggested as the



main contributors to their ice nucleating ability (Tobo et al., 2014; Hill et al., 2016). Biomass  
60 burning aerosols and fly ash also contribute to INP populations and have received increasing  
attention under global warming and the accompanying more frequent and intense wildfires (Prenni  
et al., 2012; Mccluskey et al., 2014; Umo et al., 2015). Biomass burning aerosols typically present  
lower ice nucleating ability, defined as the IN active surface site density for ice nucleation on  
particle surfaces (i.e., INP concentration/aerosol surface area concentration), compared to dust  
65 particles, while atmospheric aging can potentially enhance their ice nucleating ability (Jahl et al.,  
2021). Biogenic aerosols, such as primary biological particles composed of bacteria, pollen, fungal  
spores, and their fragments, were identified in the 1970s as important INP sources (Vali and Schnell,  
2024; Schnell and Vali, 2024). They typically can activate ice formation at a warmer temperature  
than other INPs listed above and thus may control first ice formation in clouds (Pratt et al., 2009;  
70 Creamean et al., 2013; Tobo et al., 2013). Besides these INP sources, marine aerosol (Wilson et  
al., 2015; Mccluskey et al., 2018b), secondary organic aerosol, and fuel-combustion aerosols can  
contribute to INPs (Kanji et al., 2017).

To estimate INPs for use in numerical cloud models, early parameterizations were typically based  
on empirical relationships between INPs and temperature or supersaturation alone (Bigg, 1953;  
75 Meyers et al., 1992). These parameterizations could show large biases compared to field  
observations. DeMott et al. (2010) proposed a widely used parameterization based on temperature  
and number concentrations of particles larger than 0.5  $\mu\text{m}$  in diameter, which has been applied in  
global and regional models due to its convenience and independence from detailed aerosol  
composition (Miltenberger et al., 2018; Storelvmo et al., 2011; Burrows et al., 2022). However,  
80 recent studies highlight the need for more physically based and source-specific parameterizations  
(Burrows et al., 2022; Shi and Liu, 2019; DeMott et al., 2015). Laboratory and field studies have



shown that different aerosol types (e.g., mineral dust, biological particles, marine aerosols) exhibit distinct ice-nucleating efficiencies (Hoose and Möhler, 2012; Kanji et al., 2017). Parameterizations based on the ice-nucleating IN active surface site density ( $n_s(T)$ ) have been developed for various aerosol types under immersion freezing conditions (Niemand et al., 2012; DeMott et al., 2015; Harrison et al., 2019; Mccluskey et al., 2018a; Umo et al., 2015; Schill et al., 2020; Tobo et al., 2014; O'Sullivan et al., 2014). Further field observations and laboratory studies are needed to improve these parameterizations and reduce uncertainties in INP predictions.

Mountainous regions, covering approximately one-quarter of the global land surface, play a critical role in regional and global hydrological and climatic systems. Importantly, they are sources of freshwater supporting nearly half of the world's population (Viviroli et al., 2007). Cloud and precipitation formation in mountainous areas are strongly influenced by aerosol–cloud interactions (Lynn et al., 2007). The presence, variability, and sources of INPs in mountain areas can significantly affect cloud phase, lifetime, and precipitation efficiency (Creamean et al., 2013; Lynn et al., 2007). However, INP observations in mountain environments, especially for long-term continuous measurements, are limited (Lacher et al., 2018; Sun et al., 2024; Conen et al., 2015), hampering our understanding of INP major sources, seasonal variation, and the influence of complex mountain terrain on their vertical distribution. Improved understanding of INPs in mountainous regions is essential for better representation of clouds and precipitation formation in weather and climate models, and for predicting future changes in water availability under global climate change regimes.

The Surface Atmosphere Integrated Field Laboratory (SAIL) Campaign, conducted from September 2021 to June 2023 in the Upper Colorado River Basin of the Rocky Mountains, included aims to improve understanding of how aerosols, particularly long-range transported dust



105 and wildfire smoke, affect the surface energy and water balance through their impacts on cloud, precipitation, and surface albedo, and how these effects vary by season (Feldman et al., 2023). This campaign provided a unique opportunity to investigate INPs in the Colorado Rocky Mountains over a nearly two-year period. This study presents comprehensive measurements of immersion-freezing INPs, including their seasonal and temperature-dependent variability, as well  
110 as associations with aerosol sources. We further explore different INP compositional types, biological/heat-labile, other organic, and inorganic INPs, and their inter-relationships, highlighting the importance of organic INPs. A parametrization method is proposed for INPs in this region that reproduces the observed two-year INP concentration record.

## 115 2. Methods

### 2.1 Sampling site and sample collection

The SAIL campaign deployed the Department of Energy Atmospheric Radiation Measurement (DOE ARM) Mobile Facility 2 (AMF-2) at the East River Watershed, which is located near Crested Butte and Gothic, Colorado (Feldman et al., 2023). This mountainous region, with elevations  
120 ranging from ~2440 to 4350 m above sea level, is characterized by complex terrain, a deep seasonal snowpack, and pronounced hydrometeorological gradients. The region experiences strong seasonal contrasts, with cold snowy winter and warm summers influenced by convective activity associated with the North American monsoon (Feldman et al., 2023).

For INP analyses, aerosol filter samples were collected by DOE ARM technicians through the INP  
125 Mentor Program approximately every three days from September 2021 to June 2023, with each sampling period lasting about 24 hours, as described in the instrument handbook (Creamean et al.,



2024) and repeated briefly here. Aerosols were collected on two 47 mm Nuclepore polycarbonate filters (0.2  $\mu\text{m}$  pore size) at flow rates in the range of 10–18 lpm, with total sampling volumes of approximately 15000 to 25000 L. For computing atmospheric concentrations in this study, the  
130 sampling volume was corrected to standard temperature (273.15 K) and pressure (101.3 kPa). Prior to sampling, the filters were cleaned using 10%  $\text{H}_2\text{O}_2$  and deionized (DI) water to remove organic and biological residues, then stored in sterile Petri dishes. For the first month (September 2021) of the campaign, samples were collected at the M1 site ( $38^\circ 57' 22.35''\text{N}$ ,  $106^\circ 59' 16.66''\text{W}$  at 2885 m MSL). From October 2021 to June 2023, samples were collected at the S2 site ( $38^\circ 53' 52.66''\text{N}$ ,  
135  $106^\circ 56' 35.21''\text{W}$  at 3137 m MSL). The distance between M1 and S2 sites is about 8 km. The possible difference in INP concentrations at M1 in the first month is not addressed here, since this study is aimed at representing the INPs in this region, and there was no significant change in INP concentrations when moving from the M1 to the S2 site. All samples were stored at  $-20^\circ\text{C}$  after collection, during shipment, and until the analysis in the laboratory.

140

## 2.2 Laboratory Ice Spectrometer analysis of filter-collected particles

The immersion freezing ability of particles collected on filters was quantified using the Colorado State University (CSU) Ice Nucleation Spectrometer (INS), following established procedures (Mccluskey et al., 2017; Hiranuma et al., 2015; Barry et al., 2021a), which are the same methods  
145 used by the DOE ARM INP Mentor Program (Creamean et al., 2024). The INP Mentor Program analyzed many of the samples from the SAIL campaign. Our analysis was used to fill gaps in time for the Mentor Program samples, and provide additional heat and hydrogen peroxide treatments, described below. Our data on these samples is provided within the Mentor Program data product (Shi et al., 2025). Briefly, exposed filters were mixed with 10 mL of filtered deionized water in a



150 centrifuge tube, then rotated for 20 minutes using an end-over-end shaker to resuspend the particles. Aliquots of the resuspension solution were pipetted into a 96-well PCR tray and cooled at a rate of  $0.33\text{ }^{\circ}\text{C min}^{-1}$  from room temperature to  $-30\text{ }^{\circ}\text{C}$  in the CSU INS. The number of frozen wells was recorded at  $0.5\text{ }^{\circ}\text{C}$  intervals, and INP concentrations were calculated as a function of temperature using the method of (Vali, 1971). Counting uncertainties were estimated using  
155 binomial confidence intervals (Agresti and Coull, 1998). Field blank filters were collected by exposing them at the sampling site for several seconds before removal and storage. Before calculating INP concentrations, the average number of INPs versus temperature per blank filters was subtracted from the calculated number of INPs versus temperature per sample filter, to account for potential contamination during sampling and handling, as well as any residual contamination  
160 on the filters after cleaning.

To further characterize the types of INPs, portions of the suspended aerosol solution were subjected to heat and hydrogen peroxide ( $\text{H}_2\text{O}_2$ ) treatments, followed by freezing analysis of aliquots of these portions. For heat treatment, the solution was heated to  $95\text{ }^{\circ}\text{C}$  for 21 min before measurement. This process inactivates the biological INPs by denaturation of proteins and removes heat-labile INPs  
165 (O'Sullivan et al., 2014; Tobo et al., 2014; Hill et al., 2016). In total, 43 samples were exposed to  $95\text{ }^{\circ}\text{C}$  heat treatment, and their temperature spectra are shown in Figure S1. In the peroxide treatment,  $\text{H}_2\text{O}_2$  was added to the solution and the mixture was heated at  $95\text{ }^{\circ}\text{C}$  for 21 min under UVB light to digest organics (Suski et al., 2018), and the INPs remaining were presumed to be inorganic. A total of 34 samples underwent  $\text{H}_2\text{O}_2$  treatment, with their temperature spectra shown  
170 in Figure S2. By comparing untreated (base), heat-treated, and  $\text{H}_2\text{O}_2$ -treated results, INPs were categorized into biological/heat-labile, other organic, and inorganic types. Daily et al. (2022) found that some minerals also showed reduced immersion-freezing activity after heat treatment; however,





SAIL samples showed some difference with the behaviors they reported. For minerals with initial active temperatures  $> -10^{\circ}\text{C}$ , IN active surface site density either decreased at all measured  
 175 temperatures (Arizona Test Dust (ATD) and Fluka Quartz) or was not sensitive to wet heating (K-feldspar) (Daily et al., 2022), differing from some spectra of SAIL samples that only showed decreases at warm temperatures and almost no change at temperatures  $< -18^{\circ}\text{C}$  (Figure S1). This suggests that mineral INPs have limited contributions to the decreases of INP concentrations after heat treatment in the SAIL samples.

180 There were eight ground-based sites within 55 km of the SAIL sampling locations conducted orographic cloud seeding operations by North American Weather Consultants Inc., targeting precipitation enhancement. To the best of our knowledge, these seeding stations combusted solutions in a propane flame, producing particles containing silver iodide (AgI) and other inorganic salts that served as seeding aerosols. These seeding activities occurred in specific storm situations  
 185 during winter and early spring and strongly impacted our INP observations. The measured concentrations of INPs active at temperatures from  $-7.5^{\circ}\text{C}$  to  $-27.5^{\circ}\text{C}$  for a total of 113 24-hour samples are shown in Figure S3. Since this work focuses on investigating the natural or background INPs in the Rocky Mountain region, samples collected on days that overlapped with artificial cloud seeding activities, as recorded in their logbook (data provided by North American Weather  
 190 Consultants Inc.), are highlighted in Figure S3 and excluded from the discussion below. Also, eight samples collected during winter exhibited distinct INPs spectra from other samples, but highly similar to the INP spectrum of Snomax<sup>®</sup>, a commercial non-living bacterial INP product used in snowmaking (Figure S4a). Furthermore, *P. syringae*, the bacterium type in Snomax, was identified in some of these samples based on qPCR analysis (Supplement Text S2, Figure S4b). These  
 195 samples are highly suspected to have been affected by snowmaking activities during wintertime,



associated with the location of sampling site within a ski resort at Crested Butte. Therefore, these samples, along with those affected by cloud seeding activities, were excluded from the subsequent discussion to better understand the characteristics of natural INPs in the Rocky Mountain region.

## 200    **2.3 Source apportionment**

To investigate aerosol sources in the SAIL region, source apportionment was performed using positive matrix factorization (PMF). Data from the Interagency Monitoring of Protected Visual Environments (IMPROVE) site at White River, located approximately 30 km north of the SAIL campaign site, were used for PMF analysis. The IMPROVE network (Malm et al., 1994) has  
205 collected 24-hour aerosol filter samples every three days over several decades at this site, providing a valuable dataset to understand aerosol sources and their long-term variability in the region. Chemical concentrations in the  $PM_{2.5}$  fraction of nineteen elements (Al, As, Br, Ca, Cl, Cr, Cu, Fe, K, Mg, Mn, Na, Ni, Pb, Se, Si, Ti, V, and Zn), along with nitrate, sulfate, elemental carbon (EC), organic carbon (OC), and calculated coarse mass concentrations ( $PM_{10}$ – $PM_{2.5}$  mass  
210 concentrations), from January 2014 to April 2024 were used as input for the PMF analysis performed using EPA PMF 5.0 (Norris et al., 2014). IMPROVE species concentrations were reported based on local conditions.

A five-factor solution was selected as the optimal solution. The corresponding factor profiles and time series are shown in Figures S5 and S6. These factors were identified as coarse dust, fine dust,  
215 biomass burning, sulfate-dominated, and nitrate-dominated sources. Further details on the PMF analysis and results, as well as support for their applicability over the broad surrounding Rocky



Mountain region are provided in Supplement Text S1 and Figure S7. Data for the PMF results are available through the ARM data product (Zhou et al., 2025a).

To assess the impact of different sources on INPs, the INP samples were categorized into six types based on the dominant aerosol sources during the sampling period. However, IMPROVE samples were taken only one of every three days. For days without available IMPROVE data, aerosol sources were inferred from the nearest sampling days. Samples were classified as follows: (1) Coarse dust, if coarse dust contributed more than 40% to the total  $PM_{10}$  mass concentration; (2) Biomass burning, if biomass burning accounted for more than 50% of the total  $PM_{10}$ ; (3) Dust, if the combined contribution of coarse and fine dust exceeded 50% of the total  $PM_{10}$ , with the difference between fine and coarse dust being less than 20%; (4) Fine dust, if the combined mass contribution of coarse and fine dust exceeded 50% of the  $PM_{10}$  and fine dust exceeded coarse dust by more than 20%; (5) Mixed samples, samples for which no single source was dominant, typically characterized by a sulfate contribution greater than 20% of the  $PM_{10}$ . (6) Additionally, seven samples fell within periods where more than one consecutive IMPROVE sample was missing (one week or longer). For these cases, source contributions were not interpolated, and they were categorized as samples with no source data. Source influences inferred from the nearest sampling days may introduce uncertainties. However, the merged size distribution data (section 2.5 and Figure 2) for these days showed similar size distribution patterns and comparable number concentrations for most size ranges compared to the nearest days, suggesting that significant changes in aerosol sources for these inferred days were limited. Also, the discussion is based on each group containing multiple samples, which should also reduce the uncertainties associated with the inferred source from a single sample.



## 240    **2.4 Back trajectory analysis**

Air mass back trajectory analysis was performed using the Hybrid Single-Particle Lagrangian Integrated Trajectory model (HYSPLIT; Stein et al., 2015; Rolph et al., 2017), developed by the National Oceanic and Atmospheric Administration (NOAA) Air Resources Laboratory. For each hour during each sampling period (typically 24 h), a 96-hour back trajectory was initiated at the SAIL sampling site, starting 100 m above ground level, and using the GDAS meteorological dataset with model vertical velocity. The areas traversed by the back trajectory were gridded into  $1^\circ \times 1^\circ$  cells. For each trajectory, its occurrence in each grid cell was weighted by the residence time spent in that cell. To account for the peak in occurrence near the sampling site, the residence times were further normalized by the distance from the SAIL sampling site, following the method of (Ashbaugh et al., 1985). The analysis was performed for each sample, and the resulting trajectories were aggregated to produce a composite residence-time map (Figure 1). Separate analyses were also performed for samples categorized by different source types (Figure S8), aggregating hourly trajectories for all sample times of a corresponding type across the campaign. Back trajectory data are available through the ARM data product (Zhou et al., 2025b).

255

## **2.5 Merged particle number-size distribution and IN active surface site density**

During the SAIL campaign, a scanning-mobility particle sizer (SMPS) and an optical particle counter (OPC) were deployed simultaneously with the filter sample collection to measure aerosol number size distributions in the particle diameter ranges from 10–500 nm and 0.25–35  $\mu\text{m}$ , respectively (Kuang et al., 2024; Cromwell et al., 2024). To obtain a continuous number size distribution from 10 nm to tens of micrometers, measured number size distributions from the



SMPS and OPC were merged following previous methods (Hand and Kreidenweis, 2002; Marinescu et al., 2019). Briefly, the mobility diameters from the SMPS were assumed to be equal to volume equivalent diameters by assuming the particles are spherical, and number distributions were converted to volume distributions. A scaling factor was determined by comparing the overlapping size range of the two instruments, and the OPC volume size distribution was then aligned with the SMPS volume distribution measurements by shifting OPC measured diameters to estimate the SMPS mobility diameter corresponding to that optical diameter. All aerosol data from the ARM archive were corrected to standard temperature (273.15 K) and pressure (101.3 kPa). All merged size distribution data are available through the ARM data product (Zhou et al., 2025c). A timeline of the merged number-size distributions of aerosols during the SAIL campaign is shown in Figure 2.

Assuming that the number of active ice-nucleating sites is linearly proportional to the particle surface area, the IN active surface site density ( $\text{m}^{-2}$ ) at temperature  $T$  ( $n_s(T)$ ,  $\text{m}^{-2}$ ) was calculated using the following equation:

$$n_{s,500}(T) = \frac{n_{\text{INP}}(T)}{S_{\text{m},500}} \times 10^9$$

where  $n_{\text{INP}}(T)$  ( $\text{sL}^{-1}$ ) is the measured INP concentration at temperature  $T$ ,  $S_{\text{m},500}$  ( $\mu\text{m}^2/\text{scm}^3$ ) is the surface area concentration of particles larger than 500 nm diameter calculated from the merged size distribution, assuming that particles are spherical, and the  $10^9$  conversion factor is used for  $n_{s,500}$  units of  $\text{m}^{-2}$ . In this study, the surface area of particles  $> 500$  nm is used to exclude surface area associated with pollution and other aerosol types that are inefficient sources of INPs. This is supported by the correlation found between INP concentrations and the number concentrations of particles  $> 500$  nm in a previous study (DeMott et al., 2010). The  $n_s$  is also calculated based on



total surface area concentrations to facilitate comparison with other studies and is shown in Figure  
 285 S15. While the IN active surface site density approach is typically fully justified for single INP  
 compositions, we will apply it here to the total surface areas, but also discuss adjustments needed  
 when comparing to more specific INP parameterizations.

### 3. Results and Discussion

#### 290 3.1. INPs concentrations at the SAIL study site

Samples not affected by artificial INP generation activities (cloud seeding and snowmaking  
 activities in winter; see section 2.2), representing the natural INPs in this region (84 samples in  
 total), are shown in Figure 3a. The discussion in this study focuses on these samples to better  
 understand the characteristics of natural INPs in the Rocky Mountain region. INP concentrations  
 295 ranged from  $4 \times 10^{-4} \text{ L}^{-1}$  to  $1.5 \text{ L}^{-1}$  (mean:  $0.15 \text{ L}^{-1}$ , median:  $0.05 \text{ L}^{-1}$ ) at  $-15 \text{ }^{\circ}\text{C}$ , and from  $1.2$   
 $\text{L}^{-1}$  to  $90 \text{ L}^{-1}$  (mean:  $16 \text{ L}^{-1}$ , median:  $12 \text{ L}^{-1}$ ) at  $-25 \text{ }^{\circ}\text{C}$ . Compared with previous INP studies  
 summarized by Kanji et al. (2017), the INP concentrations observed during the SAIL campaign  
 fall within the range of those in their compilation that were influenced by dust, biomass burning,  
 and precipitation, and are higher than those from marine aerosols but lower than the maximum of  
 300 those attributed to biological sources. Regarding temporal variations, INP concentrations at all  
 measured temperatures followed a similar trend over the nearly two-year observation period: low  
 in winter, increasing in spring, and reaching highest concentrations during summer and early fall.  
 For activation temperatures  $> -25 \text{ }^{\circ}\text{C}$ , the highest INP concentrations were all observed in summer.  
 For temperatures  $< -25 \text{ }^{\circ}\text{C}$ , the samples from summer also showed high INP concentrations, while  
 305 the peak concentrations occurred in September 2021. Back trajectories of those samples (2021-9-



9 and 2021-9-16) showed that the air masses mainly originated from the northwestern U.S. Intense wildfires occurred in that region during the summer of 2021 (Jain et al., 2024) and smoke plumes were transported to the SAIL site, which significantly increased aerosol loading and enhanced INPs concentrations active at low temperatures.

310 Monthly mean INP concentrations were calculated and are presented in Figure 3b, to better visualize seasonal trends and reduce the impact of individual outliers. INP concentrations showed clear seasonal variations throughout the campaign. Note that our sampling did not cover the entire month, so some outliers may have been coincidentally captured or missed, however, the two-year monthly dataset is still expected to broadly represent the seasonal variations of INPs in this region.

315 In general, INP concentrations reached peaks in June 2022 across all temperatures, and reached minimum levels during winters in both years. However, differences existed among activation temperatures. At warmer temperatures ( $-10^{\circ}\text{C}$  and  $-15^{\circ}\text{C}$ ), INP concentrations were relatively similar in warm seasons (April–October) and much higher than those in cold seasons (November–March). Bioaerosols are typically recognized as major INP sources at these activation temperatures

320 (Kanji et al., 2017), and their emissions decrease in winter in most areas (Fröhlich-Nowoisky et al., 2016). A distinct high INP peak was observed in June 2022, which was ten times higher than that in June 2023, and much higher than in other months, suggesting that a high INP emission event occurred during this month, which may be related to a specific biological emission event and/or dust event. For activation temperatures of  $-20^{\circ}\text{C}$  and  $-25^{\circ}\text{C}$ , INP concentrations also

325 showed a seasonal pattern increasing from April, peaking in June, then decreasing and reaching a minimum in December. The elevated INPs from April to September may be attributed to enhanced dust aerosols, as dust concentrations were found to increase during this period (Hand et al., 2017), as dust is a significant source of INPs, especially at lower temperatures (Kanji et al., 2017; DeMott



et al., 2015). Lower-temperature INP concentrations in June 2022 were also higher than those  
 330 in June 2023, while the magnitude of this difference (a factor of two) was less distinct from the  
 difference at  $-10^{\circ}\text{C}$  (twelve times). This suggests that the origins of INPs activated at lower  
 temperatures differ from those at warm temperatures.

### 3.2. Relationships between aerosol sources and INPs

335 The sources of aerosols to the SAIL campaign region were identified based on the PMF analysis  
 (Text S1, Figures S5 and S6). Different sources exhibited unique seasonal trends. Coarse dust  
 showed increased concentrations from April to September and had the highest annual mean  
 concentration among the five resolved particle types. Fine dust increased sharply in April, May,  
 and June, and remained low during other months. Biomass burning aerosol varied significantly by  
 340 year. Strong peaks in concentrations were observed in September 2021, with SAIL collecting some  
 samples at the end of these events, and increased contributions in June–August 2022. The biomass  
 burning factor typically showed high concentrations in summer. The sulfate-dominated and nitrate-  
 dominated factors had much lower concentrations overall, with peaks occurring in summer and  
 spring, respectively. The aerosol number size distribution also reflected the variations in different  
 345 sources. Supermicron particle concentrations were higher when coarse dust increased. Submicron  
 particles concentrations increased in September 2021 and the summer of 2022, which  
 corresponded to increases in contributions from the biomass burning factor (Figure 2). To  
 investigate the impact of different aerosol types on INPs, temporal variations between aerosol  
 sources and INP concentrations at  $-15^{\circ}\text{C}$  and  $-25^{\circ}\text{C}$  were compared, as shown in Figure S9.  
 350 Monthly average concentrations were used to minimize the impact of unsampled dates. Although  
 this may introduce uncertainties by smoothing episodic peaks of a source, the nearly two-year (22





months) record should adequately represent its seasonal cycle. Pearson correlation coefficients between monthly INP concentrations ( $-10^{\circ}\text{C}$ ,  $-15^{\circ}\text{C}$ ,  $-20^{\circ}\text{C}$ , and  $-25^{\circ}\text{C}$ ) and aerosol sources are shown in Table 1.

355 Coarse dust and biomass burning presented seasonal variations similar to those of INPs at  $-15^{\circ}\text{C}$  and  $-25^{\circ}\text{C}$ , while fine dust, nitrate-dominated, and sulfate-dominated factors had weaker correlations. The strong correlations with coarse dust and biomass burning aerosols suggest that these sources significantly contributed to observed INPs. Coarse dust showed good correlations with INPs active at all temperatures (Table 1), with correlation coefficients increasing as  
360 temperature decreased, suggesting that coarse dust is a major source of INPs, particularly at lower temperatures. This is consistent with previous findings that dust dominates the INPs at temperatures below  $-20^{\circ}\text{C}$  (Beall et al., 2022; Testa et al., 2021; Kanji et al., 2017). Interestingly, coarse dust also correlated with INPs at  $-10^{\circ}\text{C}$  ( $R^2 = 0.43$ ), a temperature range usually associated with biological INPs. This may be due to the large number of coarse dust particles, biological INPs  
365 carried on dust particles, and/or the inclusion of biological particles in the coarse dust factor, as biological particles are mostly supermicron in size (Després et al., 2012). Biomass burning presented a strong correlation with INP at  $-25^{\circ}\text{C}$  and weak correlations at warmer temperatures ( $-10^{\circ}\text{C}$  and  $-15^{\circ}\text{C}$ ), suggesting that aerosols from biomass burning contribute primarily to INPs active at lower temperatures. Combining coarse dust and biomass burning contributions showed  
370 an even better correlation with INPs (Table 1), supporting that these are the major contributors of INPs in this region, especially at lower activation temperatures.

Different from coarse dust, fine dust showed weak relationships with INPs at all temperatures ( $R^2 = 0.10\text{--}0.19$ ), suggesting lower contributions to INPs. One possible reason is that larger particles have more ice nucleation active sites (Reicher et al., 2019; DeMott et al., 2010). Another reason



375 could be differences in sources of fine and coarse dust that resulted in different ice-nucleating abilities. Fine dust presented a different seasonal pattern compared to coarse dust. Fine dust concentrations peaked in spring, especially in April, while coarse dust was higher in summer. This difference was also observed in Hand et al. (2017) for the Colorado Plateau and Central Rockies regions. They suggested that fine dust in this region is influenced by regional or long-range  
380 transported dust, such as Asian dust, while coarse aerosol mass concentrations (defined as the difference between  $PM_{10}$  and  $PM_{2.5}$ , which was almost all loaded into the coarse dust factor in our PMF analysis) are mainly derived from local and regional sources. Sulfate-dominated and nitrate-dominated sources were not correlated with INP concentrations. In remote areas, sulfate and nitrate particles mainly come from secondary formation (Seinfeld and Pandis, 2016) and are generally  
385 not considered as efficient INPs (Kanji et al., 2017).

### 3.3. INP temperature spectra categorized by sources

The total INP temperature spectra categorized by dominant aerosol types are shown in Figure 4a, and total INP spectra sorted under dominant influence of each source type are plotted separately  
390 in Figure S10. Significant differences in INP concentrations were observed between periods where different aerosol source types were dominant. Over 50% of the samples were dominated by coarse dust, which was the predominant aerosol source in this region (Figure S6). Considering that coarse dust also showed a strong correlation with INPs, this suggests INP concentrations were mainly controlled by coarse dust in this area. Mineral dust and soil dust that contains abundant organics  
395 and/or salts have been widely investigated, and are considered as important INP sources (DeMott et al., 2003; Niemand et al., 2012; Atkinson et al., 2013; DeMott et al., 2015; Pratt et al., 2010; Hamzhepour et al., 2022; Tobo et al., 2014; Steinke et al., 2016; O'Sullivan et al., 2014; Testa et



al., 2021; Pereira et al., 2022; Kanji et al., 2017). Based on back trajectories for samples categorized as coarse dust (Figure S8), air masses were mostly from local or regional sources  
400 (Central Rockies and Colorado Plateau, with additional inputs from the agricultural Imperial Valley in southern California). Considering their larger size and mass, coarse dust particles have relatively short atmospheric transport ranges, and local resuspension of soil is likely a dominant source (Hand et al., 2017). High air mass residence times were also indicated for the Great Salt Lake region, suggesting potential contributions from playa salts. This is consistent with the  
405 contributions of Cl and Na in the coarse dust factor profile from the PMF analysis (Figure S5a), and playa salt dusts have also been observed, at least at lower temperatures in the mixed phase regime, to serve as INPs (Pratt et al., 2010; Koehler et al., 2007).

Compared to INPs related to coarse dust, fine dust dominated time periods showed lower INP concentrations (Figure 4). Back trajectories also indicated different origin regions from those for  
410 coarse dust; samples dominated by fine dust had trajectories mainly from southern California and the Sonoran Desert in Arizona, known as an area with high dust emissions (Ginoux et al., 2012). Fine dust is likely long-range transported as Asian dust (Hand et al., 2017) or from the noted southwestern desert areas. Besides their different origins, the higher INP concentrations associated with coarse dust compared to fine dust can also be attributed to differences in particle size, although  
415 confirming this would require data on size-resolved INPs that were not collected. INPs related to biomass burning presented comparably high concentrations, which could be attributed to the significantly elevated aerosol loading during biomass burning events. To assess the ice nucleating activity, with the influence of aerosol concentrations and size distributions accounted for, the IN active surface site density was further investigated.

420



### 3.4. IN active surface site density ( $n_s$ ) temperature spectra

The IN active surface site density ( $n_s$ ) temperature spectra, a measure of INPs per aerosol surface area, are shown in Figure 4b for all samples, categorized by dominant aerosol type. Compared to INP concentrations, the  $n_s$  values were less variable at a given temperature, with most samples  
425 within one order of magnitude of each other, whereas INP concentrations spanned nearly two orders of magnitude, suggesting that at least some of the variability in INP concentrations can be explained by differences in particle size distributions and concentrations.

Samples dominated by a specific aerosol source (coarse dust, dust, fine dust, or biomass burning) exhibited relatively consistent  $n_s$  values with some differences among categories. The  $n_s$  of samples  
430 dominated by coarse dust was similar to or slightly higher than those having both abundant coarse and fine dust (categorized as dust), suggesting that coarse dust was the major contributor to INPs in this region. After normalizing by surface area, the  $n_s$  associated with fine dust samples showed closer values with those for coarse dust, while still lower than  $n_s$  related to coarse dust. This suggests that the lower INP concentrations in the fine dust samples can be partly attributed to  
435 differences in aerosol surface area concentrations, but also to lower active site density due to potentially different sources. The differences in  $n_s$  related to coarse dust and fine dust samples were limited, likely because there were still small contributions from coarse dust (17% on average), although fine dust dominated these samples (59% on average).

During biomass burning events, aerosol number concentrations were significantly enhanced,  
440 especially for submicron particles (Figure 2). A correlation was found between the biomass burning factor mass concentrations and the total surface area concentrations of aerosols (Figure S11), suggesting that such events significantly increased aerosol surface area concentrations. After normalization by surface area ( $S_{m,500}$ ), the  $n_s$  values associated with biomass burning were similar



to those of coarse dust. However, compared with previous studies (comparison based on total  
445 surface area), these values were higher than  $n_s$  reported from laboratory biomass burning studies  
(Umo et al., 2015; Jahn et al., 2020) and ambient biomass burning observations (Mccluskey et al.,  
2014; Barry et al., 2021b; Zhao et al., 2024). This is possible because coarse dust, which has a  
much higher  $n_s$  than biomass burning, still contributed moderately to the aerosols in these samples  
(an average of 22% of  $PM_{10}$ ), although biomass burning was the dominant aerosol source (62% on  
450 average). Wildfire events could also be a source of airborne dust (Wagner et al., 2018; Meng et al.,  
2025). From the NOAA Hazard Mapping System (Figure S12) and back trajectories (Figure S8),  
these samples were mostly affected by long-range transported biomass burning aerosols  
originating primarily from wildfires in the northwest and southwest U.S. Aging could enhance the  
 $n_s$  of biomass burning INPs (Jahl et al., 2021) and may also have contributed to higher  $n_s$  of these  
455 samples.

In contrast to the convergence observed in samples dominated by a single source, samples related  
to mixed sources showed no reduction in variability after normalization by surface area (Figure 4  
and Figure S10). Although it is difficult to precisely determine the INP sources for these samples  
based on current available analyses, this comparison strongly supports the link between INPs and  
460 the dominant bulk aerosol sources in this study.

### 3.5 Evidence of biological contribution to INPs

From the INP temperature spectra and  $n_s$  for all samples (Figure 4), the spectra for INPs active at  
temperatures  $> -18\text{ }^{\circ}\text{C}$  showed a clear segregation into two groups: one with higher INP  
465 concentrations (and  $n_s$ ) and measured detectable freezing onset temperatures mostly  $> -10\text{ }^{\circ}\text{C}$ , and



the other with lower INP concentrations (and  $n_s$ ) and lower measured detectable freezing onset temperatures, with most of those samples assigned to aerosol sources of mixed and fine dust. We found all samples in the latter group were collected from December to March. At freezing temperatures warmer than  $-18\text{ }^{\circ}\text{C}$ , biological INPs are likely to play a more important role (Kanji  
470 et al., 2017).

Here, we separated samples collected during cold seasons (December–March) and during other seasons (April–November), as shown in Figure 5. This separation clearly shows that on average, INP concentrations were lower in cold seasons, with the most striking difference at temperatures warmer than  $-15\text{ }^{\circ}\text{C}$ . A further comparison of  $n_s$  (Figure 5b) showed that samples from cold seasons  
475 had similar  $n_s$  at temperatures colder than  $-18\text{ }^{\circ}\text{C}$ . However, at warmer temperatures, samples from cold seasons showed consistently lower  $n_s$ . These results suggest that INPs that activated at temperatures colder than  $-18\text{ }^{\circ}\text{C}$  likely originated from similar sources throughout the whole year, which were primarily associated with coarse dust, as discussed above. However, in cold seasons, the contribution from biological INPs was significantly reduced, leading to the divergence in the  
480 spectra for temperatures warmer than  $-18\text{ }^{\circ}\text{C}$ . This seasonal pattern is supported by the environmental temperature dependence of biological aerosol emissions (Shawon et al., 2025).

The likely biological nature of these warmer-temperature INPs was also identified from the heat treatment of samples. A compilation of spectra from all base (untreated) analyses, heat, and  $\text{H}_2\text{O}_2$  treatments is shown in Figure 6. The difference between the base and heat spectra indicated a large  
485 contribution of heat-labile INPs at warm temperatures ( $> -18\text{ }^{\circ}\text{C}$ ), which are presumably biological INPs. Each individual heat spectrum is shown in Figure S1. In September 2021, most samples showed decreased INP concentrations at temperature warmer than  $-15\text{ }^{\circ}\text{C}$  after heat treatment, while almost no decrease was observed at lower temperatures. This reduction is likely due to



denaturing of biological INPs, reducing or removing their IN activity (Hill et al., 2016). Samples  
490 from September 2021 were strongly affected by biomass burning (Figure S6). Kobziar et al. (2024)  
found that biological aerosols can be co-emitted in biomass burning. The presence of biological  
INPs in smoke plumes was also suggested in aircraft measurements of biomass burning aerosols,  
which showed base and heat-treated spectra (Barry et al., 2021b) similar to those observed in SAIL  
samples from September and October 2022. During the SAIL campaign, Shawon et al. (2025) and  
495 Ashfiquir et al. (unpublished data) detected biological aerosols using a Wideband Integrated  
Bioaerosol Sensor (WIBS) and scanning electron microscopy during selected intensive  
observation periods (June–September 2022 and September 2022, respectively), further supporting  
the presence of biological aerosols during these periods, some of which may be active as INPs.  
There were no significant decreases in warm-temperature INP concentrations after heat treatment  
500 for samples collected from January to early April 2022 and December 2022 to March 2023,  
indicating that biological INPs concentrations were very low during the cold seasons. In the other  
seasons (April–November), many samples showed spectra in which heat treatment significantly  
decreased INP concentrations at temperatures  $> -15^{\circ}\text{C}$  and almost no change at lower  
temperatures, suggesting abundant heat-labile INPs, presumably of biological origin.

505

### 3.6 Relationships among INPs types inferred from treatments

After  $\text{H}_2\text{O}_2$  treatment, almost all samples showed significant decreases (1–2 orders of magnitude)  
in INP concentrations across all measured activation temperatures (Figure 6 and Figure S2),  
suggesting substantial contributions from organic INPs through the entire temperature spectrum.  
510 The inorganic INPs and other organic INPs were correlated at  $-15^{\circ}\text{C}$  and  $-25^{\circ}\text{C}$  (Figure 7),  
especially at the lower temperature. The correlations clustered around the 10:1 line, with ratios of



14 and 13 at  $-15^{\circ}\text{C}$  and  $-25^{\circ}\text{C}$ , respectively. These results indicated a dominant contribution from organic components suggestive of a soil origin, as previous studies found that soils contain abundant organic INPs in addition to mineral INPs (Tobo et al., 2014; O'Sullivan et al., 2014; 515 Pereira et al., 2022; Suski et al., 2018; Testa et al., 2021). A short-term observational study (DeMott et al., 2025) at the Storm Peak Laboratory in the Colorado Rockies also attributed soil INPs as the dominant INP source in late summer and early fall. These correlations provide further support that the coarse dust factor was mainly from resuspension of local or regional soil dust. Testa et al. (2021) also found a correlation at  $-25^{\circ}\text{C}$  between other organic and inorganic INPs, with a mean ratio of 520 5.5 in samples from north-central Argentina. Our results and those of Testa et al. (2021) suggest that other organic INPs and inorganic INPs are co-emitted from similar sources. The correlation coefficient increased at lower temperatures, possibly because other organic and inorganic INPs had limited contributions at  $-15^{\circ}\text{C}$ , a range strongly influenced by biological aerosols. Note that INPs from biomass burning could also contribute to this correlation, as they show similar organic 525 and inorganic INP characteristics in their INP spectra (Schill et al., 2020; Barry et al., 2021b). The only exception is sample 2021-10-14, for which similar INP concentrations were observed in the base, heat, and  $\text{H}_2\text{O}_2$  treatments at temperatures  $< -15^{\circ}\text{C}$ , suggesting that it was likely dominated by mineral dust.

Unexpectedly, a correlation was observed between the biological/heat-labile INPs and other 530 organic INPs at  $-15^{\circ}\text{C}$  ( $R^2 = 0.61$ ,  $n = 29$ , Figure 7). This correlation suggests that increases in heat-labile INPs, presumably biological INPs, were accompanied by increases in organic INPs. This is possibly because both biological and organic INPs during SAIL originated from the same source at this temperature, which was likely soil dust. However, at a warmer temperature ( $-12.5^{\circ}\text{C}$ ), the correlation was weaker ( $R^2 = 0.10$ ,  $n = 20$ ), possibly because biological INPs from





535 non-soil sources contributed at higher temperatures (Huang et al., 2021), as the ratios between biological/heat-labile INPs and other organic INPs changed from 13 ( $-15^{\circ}\text{C}$ ) to 43 ( $-12.5^{\circ}\text{C}$ ). At  $-25^{\circ}\text{C}$ , correlations between biological / heat-labile INPs and other organic INPs were much weaker, and the ratio was much lower (mean ratio of 2).

### 540 **3.7 Prediction of INPs in the Rocky Mountain region**

In this study,  $n_s$  values were found to be close to those used in the parameterizations derived from studies of agricultural soil (Tobo et al., 2014), desert dust (Niemand et al., 2012), and fertile soil (O’Sullivan et al., 2014) (Figure S13a). Applying the parameterization from Tobo et al. (2014) using the surface area of particles  $> 500\text{ nm}$  reasonably estimated INP concentrations (Figure 545 S13b), but tended to underestimate them. This is possibly because the equation provided by Tobo et al. (2014) requires an estimation of the surface area of soil particles, which introduces uncertainties when using  $S_{m,500}$ ; accurately estimating surface area of only soil particles in atmospheric samples requires additional analysis. Also, the equation from Tobo et al. (2014) is not valid for  $T > -18^{\circ}\text{C}$ . The parameterization from O’Sullivan et al. (2014) includes a wider 550 temperature range, while it tended to underestimate in temperatures warmer than  $-20^{\circ}\text{C}$  and overestimate at colder temperatures (Figure S13b). The parameterization from Niemand et al. (2012) was derived from desert dust, consisting mainly of mineral dust. Some of their dust samples might have contained arable dust or biological INPs (Beall et al., 2022). Application of their parameterization to our data showed a bias at warm temperatures (Figure S13b). Therefore, we 555 developed a parameterization based on the SAIL samples, which could be useful for estimating atmospheric INPs dominated by organic-containing soil dust.



Parameterization was based on an assumed relationship between IN active surface site density ( $n_s$ ,  $m^{-2}$ ) calculated from surface area concentrations of particles  $> 500$  nm ( $S_{m,500}$ ) and temperature ( $T$ ,  $^{\circ}C$ ) over all seasons. First, a single polynomial equation fitted to data from all samples was obtained (Figure S14), and the INP concentrations predicted from this equation and the measured  $S_{m,500}$  were compared with the measured INP concentrations (Figure S14). The predicted INPs were mostly within one order of magnitude of the measured values, suggesting this fit generally provides a reasonable estimation of INPs. However, the predicted INPs showed an overestimation trend for some samples around  $-15$   $^{\circ}C$ . This is due to the limited contribution of biological/heat-labile INPs in cold seasons.

To better represent the INP temperature spectra accounting for the seasonality of biological contributions, parameterization equations were fitted as polynomials for samples from other seasons (April–November, equation 1) and cold seasons (December–March, equation 2) separately (Figure 8), as follows,

$$\ln(n_s) = -0.007T^2 - 0.785T + 6.636 \quad (-30\text{ }^{\circ}C < T < -6\text{ }^{\circ}C) \quad (1)$$

$$\ln(n_s) = -0.030T^2 - 1.833T - 5.076 \quad (-20\text{ }^{\circ}C < T < -10\text{ }^{\circ}C) \quad (2)$$

Equation 1 was derived for most samples except those from cold seasons, and Equation 2 was obtained for samples from cold seasons (December–March). Equation 2 was constrained to intersect with Equation 1 at  $-20$   $^{\circ}C$ , as there were no significant differences at  $T < -20$   $^{\circ}C$ , and Equation 1 was used in this range. The agreement between predicted and measured INPs based on these two equations showed improvement compared to using the single equation (Figure S14), better representing the measured INPs across the full measured temperature range (Figure 8). The accurate prediction of the nearly two years of observations of INPs using this single parameterization, rather than requiring multiple  $n_s$ -based parameterizations for specific sources, is



likely due to the dominance of coarse dust as the primary INP source in this region. Note that the lack of precise parameterization for biological INPs still introduces larger uncertainties in predictions at warm temperature ranges, while applying the two-equation parameterization based on the seasonal signature of biological INPs identified in this study improves the prediction.

#### 4 Summary and atmospheric implications

This study comprehensively characterized INPs over a nearly two-year period in the mountainous Upper Colorado River Basin region. The observed average INP concentrations were  $0.15 \text{ L}^{-1}$  at  $-15^\circ\text{C}$  and  $16 \text{ L}^{-1}$  at  $-25^\circ\text{C}$ . Clear seasonal variations of INP concentrations and temperature spectra were observed, with low concentrations in winter, increasing in spring, peaking in summer, decreasing in autumn, and returning to low levels in winter. At warm activation temperatures ( $-10^\circ\text{C}$  to  $-15^\circ\text{C}$ ), some distinct peaks occurred sporadically (i.e., not observed in both years), which were mainly impacted by biological INP emission events. INPs active at colder temperatures showed more repeatable seasonal patterns and were related to the presence of dust and biomass burning aerosols.

The aerosol types in this region were identified as coarse dust, fine dust, biomass burning, sulfate-dominated, and nitrate-dominated. Coarse dust concentrations were strongly correlated with INP concentrations in all seasons and over a large temperature range, suggesting that background INPs in the study region were strongly influenced by this aerosol type. Further normalizing by surface area,  $n_s$  values supported that the identified aerosol types were related to INP sources, and that coarse dust had a significant impact on INPs. A correlation was found between the concentrations of organic and inorganic INPs observed during SAIL, indicating their similar origins. Specifically,



600 the high ratio between organic and inorganic INP types indicated that organics dominated the INPs, suggesting that organic-containing soil dust was associated with the coarse dust type and was the primary source of INPs. Back trajectories showed that coarse dust mostly originated from local or regional sources. Our results indicate that soil dust from nearby regions (e.g., the Colorado Plateau and Central Rockies), rather than long-range transported fine and mineral dust, dominates  
605 contributions to the INPs in the Upper Colorado River Basin, and therefore influences aerosol-cloud interaction and precipitation. During events in which aerosols were dominated by biomass burning, aerosol loading and total particle surface area were significantly increased. INP concentrations, especially at lower temperatures, also increased due to contributions from biomass burning aerosols and/or co-emitted dust. Fine dust, likely from long-range transport, showed a  
610 weak correlation with INP concentrations, suggesting its limited contribution to INPs.

This study also found clear evidence of biological and heat-labile INPs, which showed strong seasonal dependence. Heat-labile, presumably biological INPs were present during warm seasons but were significantly decreased in winter, consistent with the temperature dependence of biological emissions. A correlation was observed between biological/heat-labile INPs and other  
615 organic INPs at  $-15^{\circ}\text{C}$ , while the correlation is weaker at  $-12.5^{\circ}\text{C}$ . Tracking or parameterizing biological INPs using physical or chemical parameters remains a challenge in INP studies (Burrows et al., 2022). The correlation found here could provide insights for estimating biological INPs if their sources are better constrained at different active temperatures.

In this study, the origins of biological INPs are unclear due to the limitations of the analytical  
620 methods used. One possibility is that biological INPs were associated with soil dust, e.g., fungi in soil (Conen and Yakutin, 2018; O'Sullivan et al., 2016). This is supported by the correlation between biological/heat-labile INPs and other organic INPs at  $-15^{\circ}\text{C}$ . In cold seasons, snow



covers the Rocky Mountain region and inhibits the suspension of local soil dust, which is considered as the main source of INPs in this region. This assumption that coarse dust emissions  
625 are suppressed in cold seasons is also supported by the observation that more than half of the samples in cold seasons were dominated by mixed sources and fine dust, instead of coarse dust. However, the correlation between biological/heat-labile INPs and other organic INPs was weaker ( $R^2 = 0.10$ ) at a warmer temperature ( $-12.5^\circ\text{C}$ ). This suggests that there are contributions from other biological INPs (e.g., those originating from vegetation) at warmer freezing temperatures,  
630 which are likely independent of soil dust emissions, thereby complicating the estimation of biological INPs. In this case, the INP spectra in cold seasons likely represent that of soil dust, and the spectra in other seasons represent the combination of soil dust and biological INPs. In future studies, identifying whether biological INPs originate from vegetation, from soil-associated sources, or from a combination of both, and clarifying their relative contributions, would help  
635 improve our understanding of biological INP variability and could potentially improve their estimation.

Based on the seasonal variation of heat-labile and biological INPs, two separate parameterization equations based on IN active surface site density were developed for warm and cold seasons. These equations well estimated the measured INP concentrations across the measured temperature and  
640 concentration ranges. The parameterization developed here could be useful for representing INPs from organic-containing soil dust in other mountain regions. Furthermore, the INP concentrations in this study were similar to those observed in ambient samples influenced by agricultural soil in Argentina (Testa et al., 2021). The  $n_s$  values reported for agricultural soil samples (Tobo et al., 2014) were higher than those calculated from total surface area (Figure S15), but similar to  $n_s$  when  
645 based on surface area of particles  $> 500\text{ nm}$  (Figure S13). This finding suggests that using particles  $>$



500 nm is a reasonable threshold for excluding most aerosol types that are inefficient INP sources, and approximating aerosol surface area contributions from organic-containing soils. Since SAIL was conducted at a remote site in the Rocky Mountains, these comparisons suggest that the parameterization developed in this study can potentially be applied to other remote continental areas. A recent global modeling study (Herbert et al., 2025) found that including organic INP components in dust particles, which are present in many soils, can significantly improve predictive accuracy. It is therefore essential to validate the INPs originating from organic-containing soil dust, beyond the mineral dust that has already been intensively studied, through field measurements across different continental regions.

### Data Availability

The data from the SAIL campaign used in this study are available through the ARM Data Discovery (<https://adc.arm.gov/discovery/>). This includes INPs data (Shi et al., 2025), source apportionment results (Zhou et al., 2025a), back trajectory data (Zhou et al., 2025b), merged aerosol number-size distribution (Zhou et al., 2025c), and particle number size distribution data from SMPS (Kuang et al., 2024) and OPC (Cromwell et al., 2024).

### Author contributions

RP, SK, PD, and RZ conceptualized the study. DJ, RZ, KA, and OD performed additional immersion-mode INP measurements. RZ, RP and SK conducted the source apportionment and merged the size distribution data. RZ, RP, KA and SK performed the back trajectory analysis. KB



performed qPCR analysis. RZ wrote the manuscript, with revisions from RP, PD, and SK. All authors reviewed the manuscript and contributed to the final version of the manuscript.

## 670    **Competing interests**

The authors declare no competing interests.

## **Acknowledgements**

This work is supported by DOE Atmospheric Systems Research award DE-SC0024202. We thank  
675 the DOE ARM INP Mentors Jessie Creamean, Tom Hill, and Carson Hume for coordinating the  
sample collections and for helping with the combined INP data archival. We also thank Ty Johnson  
for assistance with generating the NOAA Hazard Mapping System plots. The authors acknowledge  
the NOAA Air Resources Laboratory (ARL) for the provision of the HYSPLIT transport and  
dispersion model used in this publication. We also thank the Interagency Monitoring of Protected  
680 Visual Environments (IMPROVE) network for providing aerosol composition data. IMPROVE is  
a collaborative association of state, tribal, and federal agencies, and international partners. US  
Environmental Protection Agency is the primary funding source, with contracting and research  
support from the National Park Service. The Air Quality Group at the University of California,  
Davis is the central analytical laboratory, with ion analysis provided by Research Triangle Institute,  
685 and carbon analysis provided by Desert Research Institute. We thank North American Weather  
Consultants Inc. for providing records of their cloud seeding activities near the SAIL campaign  
site. Kelton Ayars and Oren Dutton would like to acknowledge support from the Scott  
Undergraduate Research Experiences program at Colorado State University.

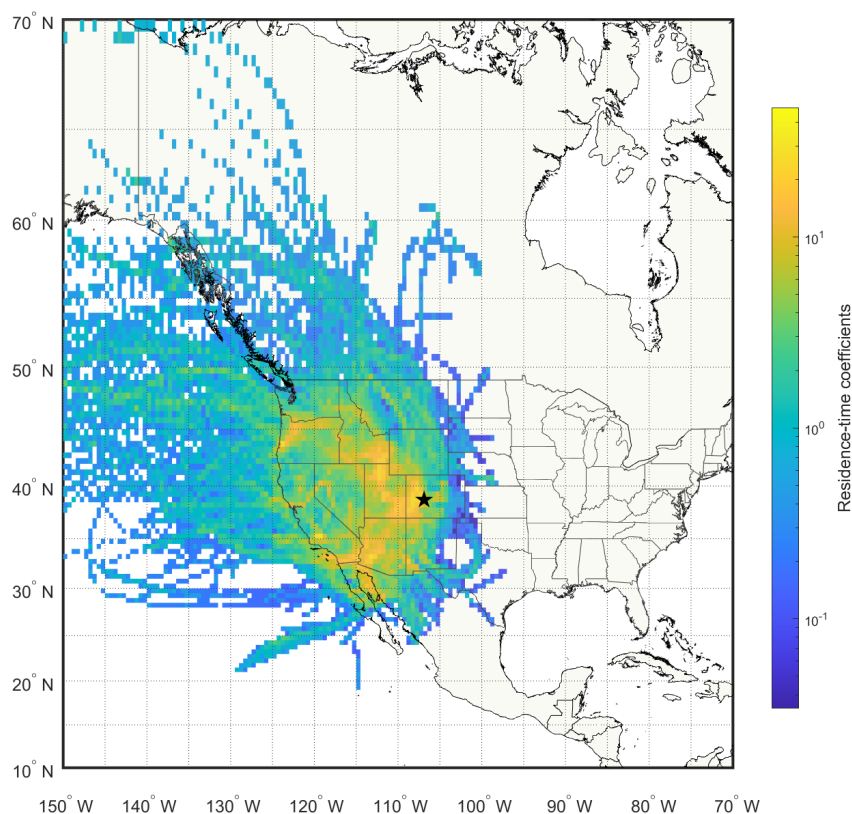


**Figure 1.** Residence-time weighted back trajectories for all sampling periods. 96-hour back trajectories were generated hourly during each sampling period and normalized by residence time and distance from the sampling site. The residence-time coefficients indicate the relative time air masses spent within each grid cell. The black star marks the SAIL sampling location.



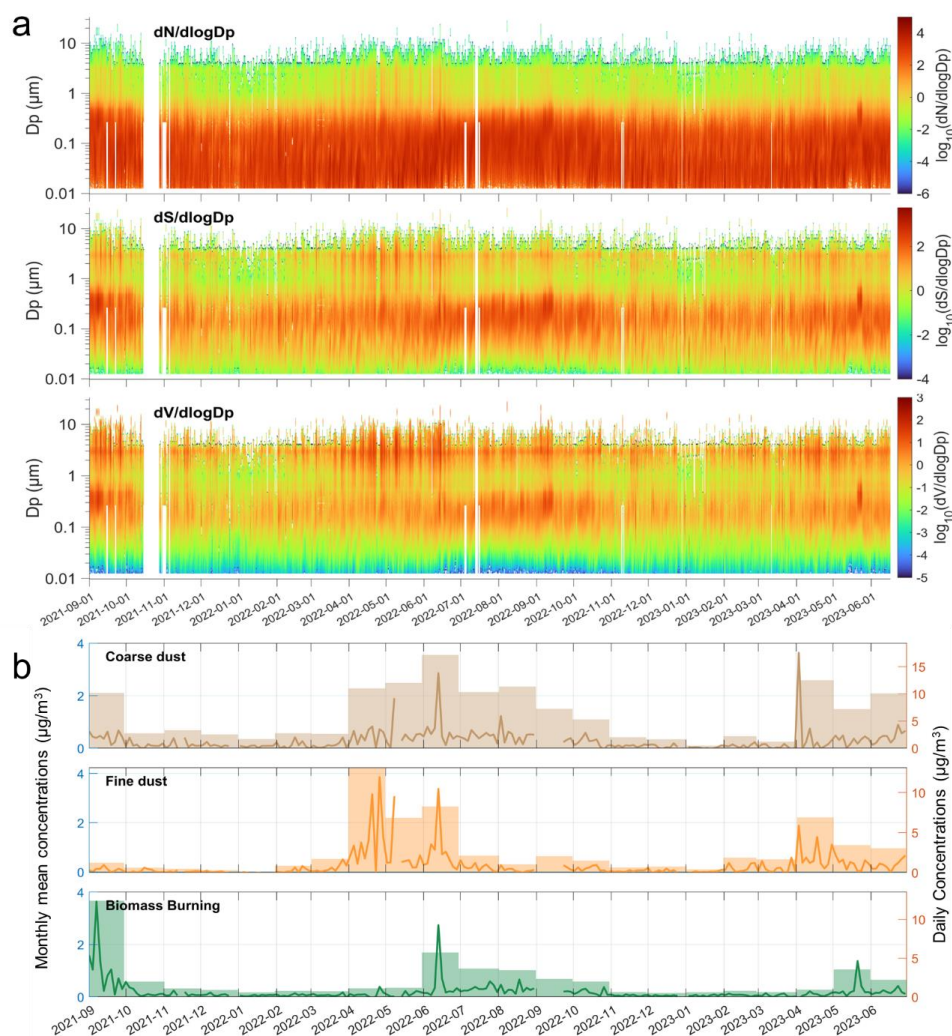


**Figure 2.** (a) Number size distribution ( $dN/d\log D_p$ ,  $\text{scm}^{-3}$ ), surface area size distribution ( $dS/d\log D_p$ ,  $\mu\text{m}^2/\text{scm}^{-3}$ ), and volume size distribution ( $dV/d\log D_p$ ,  $\mu\text{m}^3/\text{scm}^{-3}$ ), derived from merged size distribution assuming spherical particles during the SAIL campaign. (b) Time series of aerosol mass concentrations ( $\mu\text{g m}^{-3}$ ) of coarse dust, fine dust, and biomass burning. Lines and bars represent daily and monthly mean concentrations, respectively.

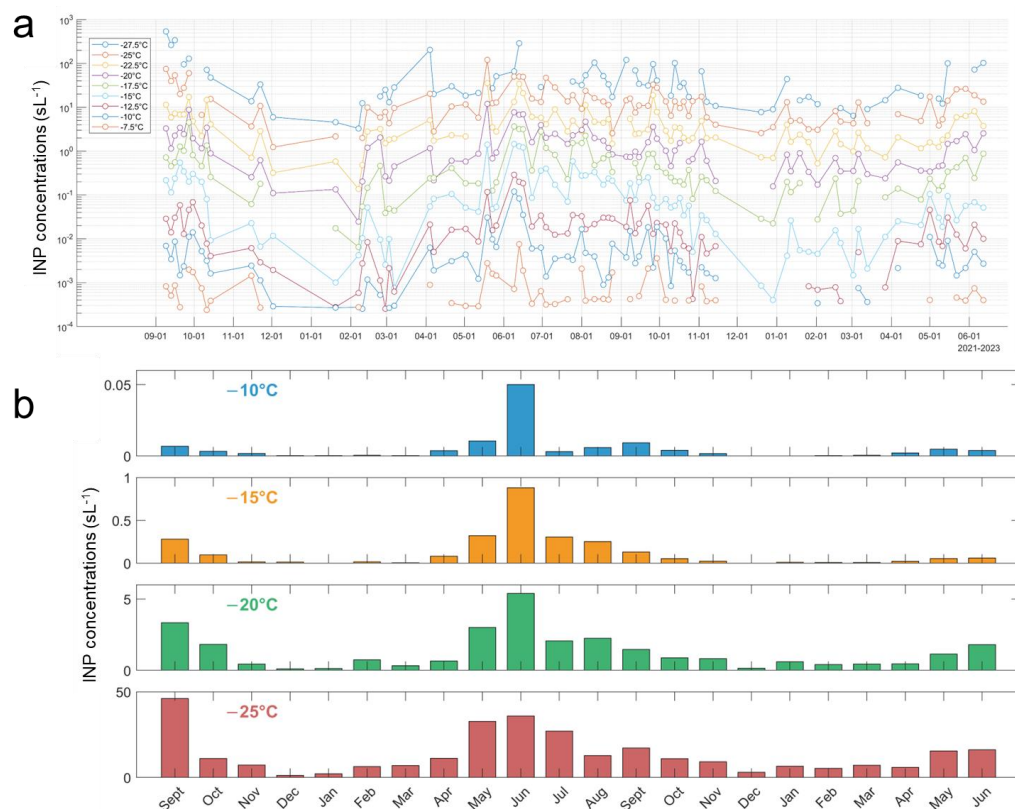


**Figure 3.** Measured INP concentrations (sL<sup>-1</sup>) during the SAIL campaign (September 2021–June 2023), excluding samples obtained during cloud seeding and snowmaking activities. (a) INP concentrations at temperatures from -7.5 °C to -27.5 °C in 2.5°C intervals. (b) Monthly mean INP concentrations at temperatures of -10 °C, -15 °C, -20 °C, and -25 °C.

705

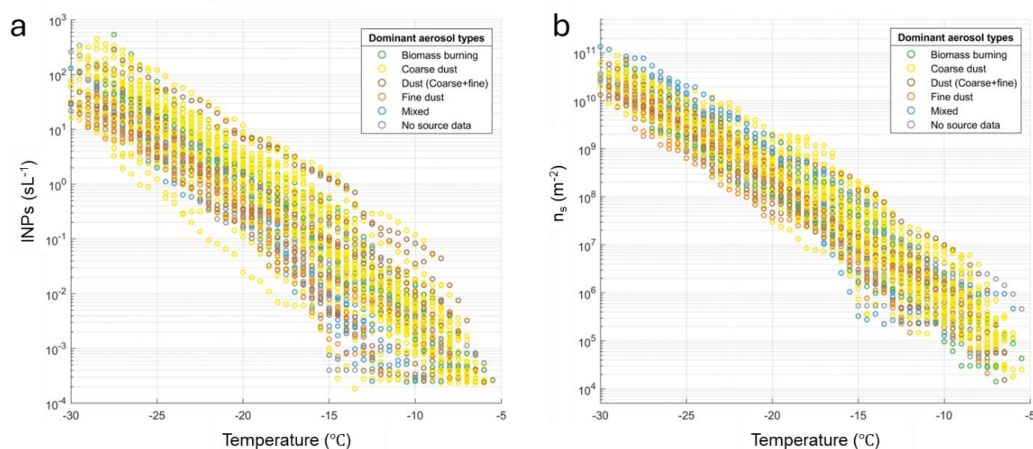


**Figure 4.** (a) Total INP concentration ( $\text{sL}^{-1}$ ) temperature spectra, and (b) IN active surface site density ( $n_s$ ,  $\text{m}^{-2}$ ) calculated based on the surface area of particles larger than 500 nm. All samples were categorized by the dominant aerosol sources. Colors in the legend represent the dominant aerosol types during sampling.

710

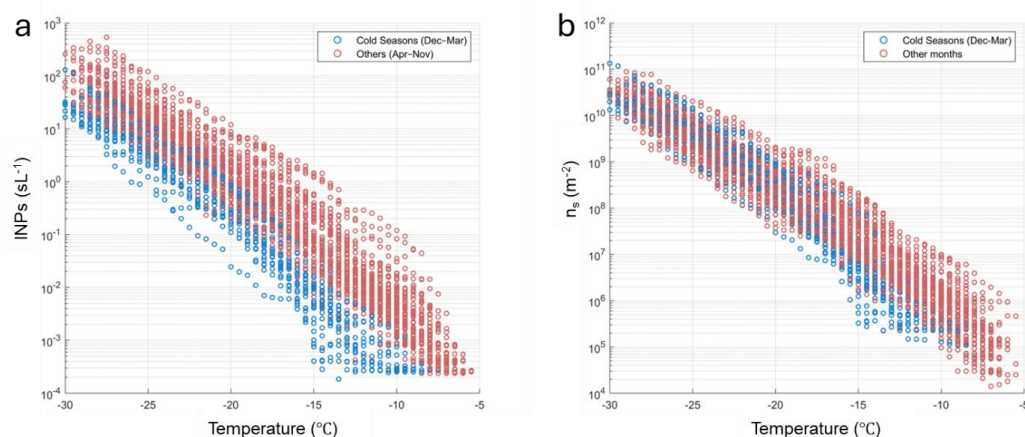


**Figure 5.** (a) INP temperature spectra and (b) IN active surface site density ( $n_s$ ) categorized by sampling date as cold seasons (December–March) and other seasons (April–November).  $n_s$  was calculated based on the surface area of particles larger than 500 nm.

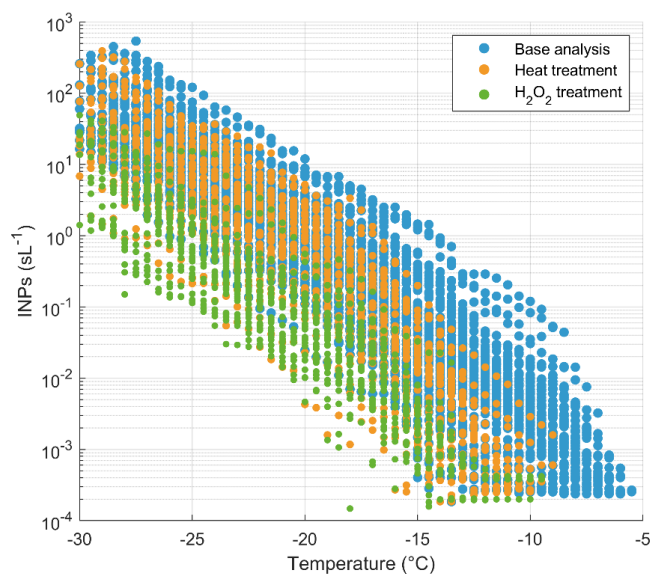


**Figure 6.** Comparison of INP temperature spectra from base (untreated), heat-treated, and H<sub>2</sub>O<sub>2</sub>-  
 720 treated analyses.

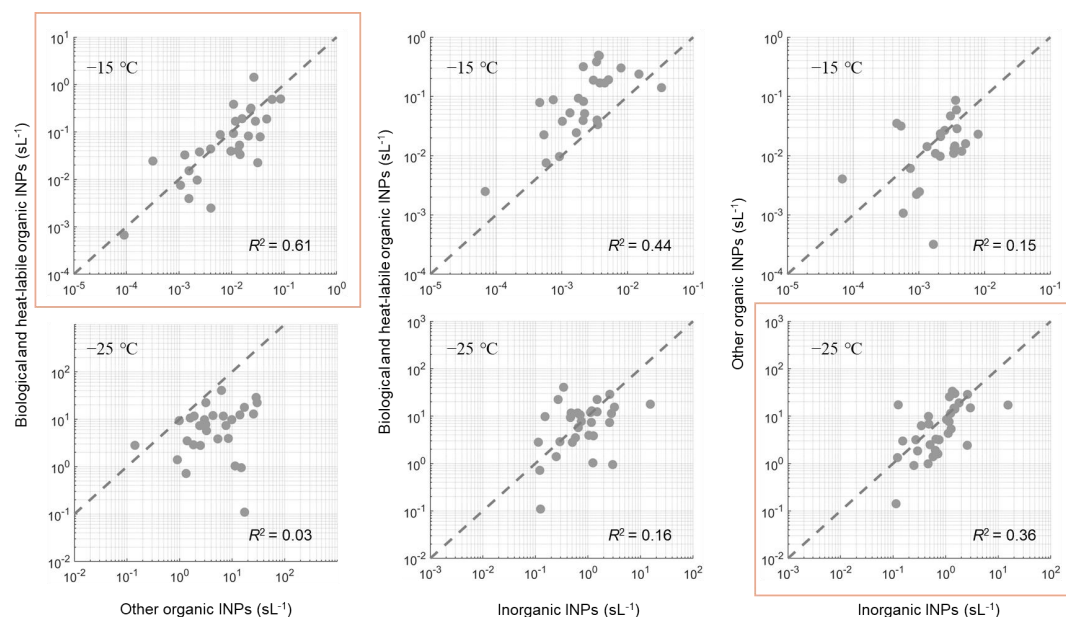


**Figure 7.** The correlations between concentrations of biological and heat-labile INPs, other organic INPs, and inorganic INPs active at temperatures of  $-15^{\circ}\text{C}$  (upper row) and  $-25^{\circ}\text{C}$  (lower row). Dashed lines show 10:1 correlation for reference. The rectangles show the highest correlations at each temperature.

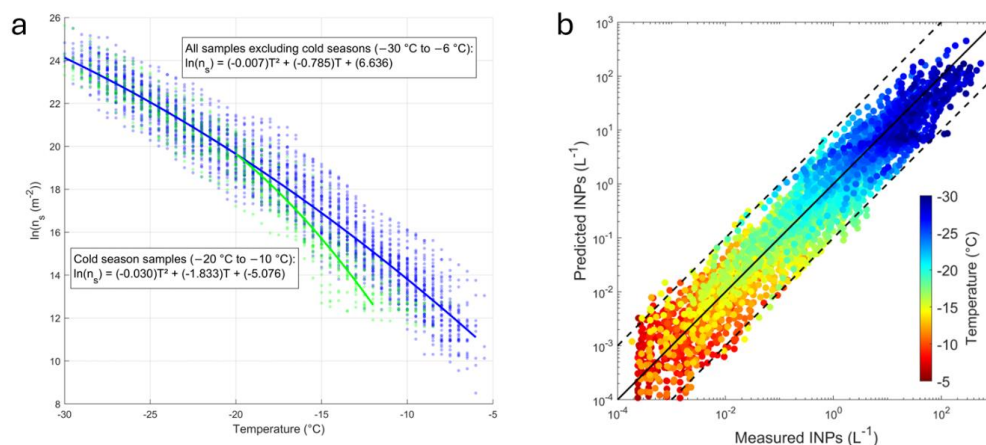


**Figure 8.** (a) All cold season (December–March) and other seasons (April–November) INP data, expressed as IN active surface site density  $n_s$  (based on the surface area of particles larger than 500 nm), with parameterization fits. All samples, excluding those from cold seasons, were used to develop the parameterization equation for temperatures from  $-30^{\circ}\text{C}$  to  $-6^{\circ}\text{C}$ . A separate equation was developed for samples from cold seasons at temperatures from  $-20^{\circ}\text{C}$  to  $-10^{\circ}\text{C}$ . (b) Comparison between predicted INP concentrations based on the parameterization equations and measured surface area concentrations, and measured INP concentrations.





**Table 1.** Pearson correlation coefficients ( $R^2$ ) between monthly means of INP concentrations and source factor concentrations.

	Coarse dust	Fine dust	Biomass burning	Sulfate-dominated	Nitrate-dominated	Coarse dust and biomass burning
-10 °C	0.430*	0.192	0.157	0.070	0.036	0.389*
-15 °C	0.568*	0.175	0.316*	0.093	0.040	0.590*
-20 °C	0.579*	0.117	0.484*	0.121	0.040	0.706*
-25 °C	0.500*	0.100	0.688*	0.147	0.051	0.763*

\*  $p < 0.01$





## 740 References

- Agresti, A. and Coull, B. A.: Approximate is better than “exact” for interval estimation of binomial proportions, *Am. Stat.*, 52, 119-126, 1998.
- Ashbaugh, L. L., Malm, W. C., and Sadeh, W. Z.: A residence time probability analysis of sulfur concentrations at Grand Canyon National Park, *Atmos. Environ.*, 19, 1263-1270, 1985.
- 745 Atkinson, J. D., Murray, B. J., Woodhouse, M. T., Whale, T. F., Baustian, K. J., Carslaw, K. S., Dobbie, S., O'Sullivan, D., and Malkin, T. L.: The importance of feldspar for ice nucleation by mineral dust in mixed-phase clouds, *Nature*, 498, 355-358, <https://doi.org/10.1038/nature12278>, 2013.
- Barry, K. R., Hill, T. C. J., Jentzsch, C., Moffett, B. F., Stratmann, F., and DeMott, P. J.: Pragmatic protocols for working cleanly when measuring ice nucleating particles, *Atmos. Res.*, 250, <https://doi.org/10.1016/j.atmosres.2020.105419>, 2021a.
- 750 Barry, K. R., Hill, T. C. J., Levin, E. J. T., Twohy, C. H., Moore, K. A., Weller, Z. D., Toohey, D. W., Reeves, M., Campos, T., Geiss, R., Schill, G. P., Fischer, E. V., Kreidenweis, S. M., and DeMott, P. J.: Observations of Ice Nucleating Particles in the Free Troposphere From Western US Wildfires, *J. Geophys. Res: Atmos.*, 126, <https://doi.org/10.1029/2020jd033752>, 2021b.
- 755 Beall, C. M., Hill, T. C. J., DeMott, P. J., Köneman, T., Pikridas, M., Drewnick, F., Harder, H., Pöhlker, C., Lelieveld, J., Weber, B., Iakovides, M., Prokes, R., Sciare, J., Andreae, M. O., Stokes, M. D., and Prather, K. A.: Ice-nucleating particles near two major dust source regions, *Atmos. Chem. Phys.*, 22, 12607-12627, <https://doi.org/10.5194/acp-22-12607-2022>, 2022.
- 760 Bigg, E. K.: The supercooling of water, *Proceedings of the Physical Society. Section B*, 66, 688, 1953.
- Burrows, S. M., McCluskey, C. S., Cornwell, G., Steinke, I., Zhang, K., Zhao, B., Zawadowicz, M., Raman, A., Kulkarni, G., and China, S.: Ice-nucleating particles that impact clouds and climate: Observational and modeling research needs, *Rev. Geophys.*, 60, e2021RG000745, 2022.
- 765 Conen, F. and Yakutin, M. V.: Soils rich in biological ice-nucleating particles abound in ice-nucleating macromolecules likely produced by fungi, *Biogeosciences*, 15, 4381-4385, <https://doi.org/10.5194/bg-15-4381-2018>, 2018.
- Conen, F., Rodríguez, S., Hülin, C., Henne, S., Herrmann, E., Bukowiecki, N., and Alewell, C.: Atmospheric ice nuclei at the high-altitude observatory Jungfraujoch, Switzerland, *Tellus B Chem. Phys. Meteorol.*, 67, 25014, 2015.
- 770 Creamean, J. M., Hill, T. C., Hume, C. C., and Devadoss, T.: Ice Nucleation Spectrometer (INS) Instrument Handbook, Oak Ridge National Laboratory (ORNL), Oak Ridge, TN (United States) Atmospheric Radiation Measurement (ARM) Data Center, <https://doi.org/10.2172/1846263>, 2024.
- 775 Creamean, J. M., Suski, K. J., Rosenfeld, D., Cazorla, A., DeMott, P. J., Sullivan, R. C., White, A. B., Ralph, F. M., Minnis, P., and Comstock, J. M.: Dust and biological aerosols from the Sahara and Asia influence precipitation in the western US, *Science*, 339, 1572-1578, 2013.
- Cromwell, E., Singh, A., & Kuang, C. Optical Particle Counter (AOSOPC), 2021-10-27 to 2023-06-16, ARM Mobile Facility (GUC), Gunnison, CO; Supplemental Facility 2 (S2). Atmospheric



- 780 Radiation Measurement (ARM) User Facility. <https://doi.org/10.5439/1824224>, Data accessed 2024-08-01.
- de Boer, G., Morrison, H., Shupe, M. D., and Hildner, R.: Evidence of liquid dependent ice nucleation in high-latitude stratiform clouds from surface remote sensors, *Geophys. Res. Lett.*, 38, 2011.
- 785 DeMott, P. J., Sassen, K., Poellot, M. R., Baumgardner, D., Rogers, D. C., Brooks, S. D., Prenni, A. J., and Kreidenweis, S. M.: African dust aerosols as atmospheric ice nuclei, *Geophys. Res. Lett.*, 30, <https://doi.org/10.1029/2003gl017410>, 2003.
- DeMott, P. J., Prenni, A. J., Liu, X., Kreidenweis, S. M., Petters, M. D., Twohy, C. H., Richardson, M. S., Eidhammer, T., and Rogers, D. C.: Predicting global atmospheric ice nuclei distributions and their impacts on climate, *Proc. Natl. Acad. Sci. USA*, 107, 11217-11222, <https://doi.org/10.1073/pnas.0910818107>, 2010.
- 790 DeMott, P. J., Prenni, A. J., McMeeking, G. R., Sullivan, R. C., Petters, M. D., Tobo, Y., Niemand, M., Möhler, O., Snider, J. R., Wang, Z., and Kreidenweis, S. M.: Integrating laboratory and field data to quantify the immersion freezing ice nucleation activity of mineral dust particles, *Atmos. Chem. Phys.*, 15, 393-409, <https://doi.org/10.5194/acp-15-393-2015>, 2015.
- 795 DeMott, P. J., Mirrielees, J. A., Petters, S. S., Cziczo, D. J., Petters, M. D., Bingemer, H. G., Hill, T. C. J., Froyd, K., Garimella, S., Hallar, A. G., Levin, E. J. T., McCubbin, I. B., Perring, A. E., Rapp, C. N., Schiebel, T., Schrod, J., Suski, K. J., Weber, D., Wolf, M. J., Zawadowicz, M., Zenker, J., Möhler, O., and Brooks, S. D.: Field intercomparison of ice nucleation measurements: the Fifth International Workshop on Ice Nucleation Phase 3 (FIN-03), *Atmos. Meas. Tech.*, 18, 639-672, <https://doi.org/10.5194/amt-18-639-2025>, 2025.
- 800 Després, V., Huffman, J. A., Burrows, S. M., Hoose, C., Safatov, A., Buryak, G., Fröhlich-Nowoisky, J., Elbert, W., Andreae, M., Pöschl, U., and Jaenicke, R.: Primary biological aerosol particles in the atmosphere: a review, *Tellus B Chem. Phys. Meteorol.*, 64, 15598, <https://doi.org/10.3402/tellusb.v64i0.15598>, 2012.
- 805 Feldman, D. R., Aiken, A. C., Boos, W. R., Carroll, R. W. H., Chandrasekar, V., Collis, S., Creamean, J. M., de Boer, G., Deems, J., DeMott, P. J., Fan, J., Flores, A. N., Gochis, D., Grover, M., Hill, T. C. J., Hodshire, A., Hulm, E., Hume, C. C., Jackson, R., Junyent, F., Kennedy, A., Kumjian, M., Levin, E. J. T., Lundquist, J. D., O'Brien, J., Raleigh, M. S., Reithel, J., Rhoades, A., Rittger, K., Rudisill, W., Sherman, Z., Siirila-Woodburn, E., Skiles, S. M., Smith, J. N., Sullivan, R. C., Theisen, A., Tuftedal, M., Varble, A. C., Wiedlea, A., Wielandt, S., Williams, K., and Xu, Z.: The Surface Atmosphere Integrated Field Laboratory (SAIL) Campaign, *Bull. Amer. Meteor. Soc.*, 104, E2192-E2222, <https://doi.org/10.1175/bams-d-22-0049.1>, 2023.
- 810 Fröhlich-Nowoisky, J., Kampf, C. J., Weber, B., Huffman, J. A., Pöhlker, C., Andreae, M. O., Lang-Yona, N., Burrows, S. M., Gunthe, S. S., and Elbert, W.: Bioaerosols in the Earth system: Climate, health, and ecosystem interactions, *Atmos. Res.*, 182, 346-376, 2016.
- 815 Garcia, E., Hill, T. C., Prenni, A. J., DeMott, P. J., Franc, G. D., and Kreidenweis, S. M.: Biogenic ice nuclei in boundary layer air over two US High Plains agricultural regions, *J. Geophys. Res: Atmos.*, 117, 2012.



- 820 Ginoux, P., Prospero, J. M., Gill, T. E., Hsu, N. C., and Zhao, M.: Global-scale attribution of anthropogenic and natural dust sources and their emission rates based on MODIS Deep Blue aerosol products, *Rev. Geophys.*, 50, <https://doi.org/10.1029/2012rg000388>, 2012.
- Hamzhepour, N., Marcolli, C., Klumpp, K., Thöny, D., and Peter, T.: The Urmia playa as a source of airborne dust and ice-nucleating particles – Part 2: Unraveling the relationship between soil dust composition and ice nucleation activity, *Atmos. Chem. Phys.*, 22, 14931-14956, <https://doi.org/10.5194/acp-22-14931-2022>, 2022.
- 825 Hand, J. L. and Kreidenweis, S. M.: A New Method for Retrieving Particle Refractive Index and Effective Density from Aerosol Size Distribution Data, *Aerosol Sci. Technol.*, 36, 1012-1026, <https://doi.org/10.1080/02786820290092276>, 2002.
- 830 Hand, J. L., Gill, T. E., and Schichtel, B. A.: Spatial and seasonal variability in fine mineral dust and coarse aerosol mass at remote sites across the United States, *J. Geophys. Res: Atmos.*, 122, 3080-3097, <https://doi.org/10.1002/2016jd026290>, 2017.
- Harrison, A. D., Lever, K., Sanchez-Marroquin, A., Holden, M. A., Whale, T. F., Tarn, M. D., McQuaid, J. B., and Murray, B. J.: The ice-nucleating ability of quartz immersed in water and its atmospheric importance compared to K-feldspar, *Atmos. Chem. Phys.*, 19, 11343-11361, <https://doi.org/10.5194/acp-19-11343-2019>, 2019.
- 835 Herbert, R. J., Sanchez-Marroquin, A., Grosvenor, D. P., Pringle, K. J., Arnold, S. R., Murray, B. J., and Carslaw, K. S.: Gaps in our understanding of ice-nucleating particle sources exposed by global simulation of the UK Earth System Model, *Atmos. Chem. Phys.*, 25, 291-325, 2025.
- 840 Hill, T. C. J., DeMott, P. J., Tobo, Y., Fröhlich-Nowoisky, J., Moffett, B. F., Franc, G. D., and Kreidenweis, S. M.: Sources of organic ice nucleating particles in soils, *Atmos. Chem. Phys.*, 16, 7195-7211, <https://doi.org/10.5194/acp-16-7195-2016>, 2016.
- Hiranuma, N., Augustin-Bauditz, S., Bingemer, H., Budke, C., Curtius, J., Danielczok, A., Diehl, K., Dreischmeier, K., Ebert, M., Frank, F., Hoffmann, N., Kandler, K., Kiselev, A., Koop, T., 845 Leisner, T., Möhler, O., Nillius, B., Peckhaus, A., Rose, D., Weinbruch, S., Wex, H., Boose, Y., DeMott, P. J., Hader, J. D., Hill, T. C. J., Kanji, Z. A., Kulkarni, G., Levin, E. J. T., McCluskey, C. S., Murakami, M., Murray, B. J., Niedermeier, D., Petters, M. D., O'Sullivan, D., Saito, A., Schill, G. P., Tajiri, T., Tolbert, M. A., Welti, A., Whale, T. F., Wright, T. P., and Yamashita, K.: A comprehensive laboratory study on the immersion freezing behavior of illite NX particles: a comparison of 17 ice nucleation measurement techniques, *Atmos. Chem. Phys.*, 15, 2489-2518, <https://doi.org/10.5194/acp-15-2489-2015>, 2015.
- 850 Hoose, C. and Möhler, O.: Heterogeneous ice nucleation on atmospheric aerosols: a review of results from laboratory experiments, *Atmos. Chem. Phys.*, 12, 9817-9854, <https://doi.org/10.5194/acp-12-9817-2012>, 2012.
- 855 Huang, S., Hu, W., Chen, J., Wu, Z. J., Zhang, D. Z., and Fu, P. Q.: Overview of biological ice nucleating particles in the atmosphere, *Environ. Int.*, 146, <https://doi.org/10.1016/j.envint.2020.106197>, 2021.
- IPCC, 2022: Climate Change 2022: Impacts, Adaptation, and Vulnerability., Contribution of Working Group II to the Sixth Assessment Report of the Intergovernmental Panel on Climate Change [H.-O. Pörtner, D.C. Roberts, M. Tignor, E.S. Poloczanska, K. Mintenbeck, A. Alegría, 860 M. Craig, S. Langsdorf, S. Löschke, V. Möller, A. Okem, B. Rama (eds.)]. Cambridge University



- Press. Cambridge University Press, Cambridge, UK and New York, NY, USA, 3056 pp.,  
<https://doi.org/10.1017/9781009325844>, 2022.
- 865 Jahl, L. G., Brubaker, T. A., Polen, M. J., Jahn, L. G., Cain, K. P., Bowers, B. B., Fahy, W. D.,  
 Graves, S., and Sullivan, R. C.: Atmospheric aging enhances the ice nucleation ability of  
 biomass-burning aerosol, *Sci. Adv.*, 7, eabd3440, 2021.
- Jahn, L. G., Jahl, L. G., Bland, G. D., Bowers, B. B., Monroe, L. W., and Sullivan, R. C.:  
 Metallic and crustal elements in biomass-burning aerosol and ash: Prevalence, significance, and  
 similarity to soil particles, *ACS Earth Space Chem.*, 5, 136-148, 2020.
- 870 Jain, P., Sharma, A. R., Acuna, D. C., Abatzoglou, J. T., and Flannigan, M.: Record-breaking fire  
 weather in North America in 2021 was initiated by the Pacific northwest heat dome, *Commun.*  
*Earth Environ.*, 5, 202, 2024.
- Kanji, Z. A., Ladino, L. A., Wex, H., Boose, Y., Burkert-Kohn, M., Cziczo, D. J., and Krämer,  
 M.: Overview of Ice Nucleating Particles, *Meteor. Monogr.*, 58, 1.1-1.33,  
 875 <https://doi.org/10.1175/amsmonographs-d-16-0006.1>, 2017.
- Kiselev, A., Bachmann, F., Pedevilla, P., Cox, S. J., Michaelides, A., Gerthsen, D., and Leisner,  
 T.: Active sites in heterogeneous ice nucleation-the example of K-rich feldspars, *Science*, 355,  
 367-371, <https://doi.org/10.1126/science.aai8034>, 2017.
- Knippertz, P. and Stuut, J.-B. W.: Mineral dust, Mineral dust—A key player in the Earth system,  
 880 121-147, Springer, 2014.
- Kobziar, L. N., Lampman, P., Tohidi, A., Kochanski, A. K., Cervantes, A., Hudak, A. T.,  
 McCarley, R., Gullett, B., Aurell, J., and Moore, R.: Bacterial emission factors: a foundation for  
 the terrestrial-atmospheric modeling of bacteria aerosolized by wildland fires, *Environ. Sci.*  
*Technol.*, 58, 2413-2422, 2024.
- 885 Koehler, K. A., Kreidenweis, S. M., DeMott, P. J., Prenni, A. J., and Petters, M. D.: Potential  
 impact of Owens (dry) Lake dust on warm and cold cloud formation, *J. Geophys. Res: Atmos.*,  
 112, 2007.
- Kuang, C., Singh, A., Howie, J., Salwen, C., & Hayes, C. Scanning mobility particle sizer  
 (AOSSMPS), 2021-10-27 to 2023-06-16, ARM Mobile Facility (GUC), Gunnison, CO;  
 890 Supplemental Facility 2 (S2). Atmospheric Radiation Measurement (ARM) User Facility.  
<https://doi.org/10.5439/1476898>, Data accessed 2024-08-01.
- Lacher, L., Steinbacher, M., Bukowiecki, N., Herrmann, E., Zipori, A., and Kanji, Z. A.: Impact  
 of Air Mass Conditions and Aerosol Properties on Ice Nucleating Particle Concentrations at the  
 High Altitude Research Station Jungfraujoch, *Atmosphere*, 9,  
 895 <https://doi.org/10.3390/atmos9090363>, 2018.
- Lohmann, U. and Feichter, J.: Global indirect aerosol effects: a review, *Atmos. Chem. Phys.*, 5,  
 715-737, <https://doi.org/10.5194/acp-5-715-2005>, 2005.
- Lynn, B., Khain, A., Rosenfeld, D., and Woodley, W. L.: Effects of aerosols on precipitation from  
 orographic clouds, *J. Geophys. Res: Atmos.*, 112, 2007.
- 900 Malm, W. C., Sisler, J. F., Huffman, D., Eldred, R. A., and Cahill, T. A.: Spatial and seasonal  
 trends in particle concentration and optical extinction in the United States, *J. Geophys. Res:*  
*Atmos.*, 99, 1347-1370, 1994.



- Marinescu, P. J., Levin, E. J., Collins, D., Kreidenweis, S. M., and van den Heever, S. C.: Quantifying aerosol size distributions and their temporal variability in the Southern Great Plains, USA, *Atmos. Chem. Phys.*, 19, 11985-12006, 2019.
- McCluskey, C. S., DeMott, P. J., Prenni, A. J., Levin, E. J. T., McMeeking, G. R., Sullivan, A. P., Hill, T. C. J., Nakao, S., Carrico, C. M., and Kreidenweis, S. M.: Characteristics of atmospheric ice nucleating particles associated with biomass burning in the US: Prescribed burns and wildfires, *J. Geophys. Res: Atmos.*, 119, 10458-10470, <https://doi.org/10.1002/2014jd021980>, 2014.
- McCluskey, C. S., Ovadnevaite, J., Rinaldi, M., Atkinson, J., Belosi, F., Ceburnis, D., Marullo, S., Hill, T. C. J., Lohmann, U., Kanji, Z. A., O'Dowd, C., Kreidenweis, S. M., and DeMott, P. J.: Marine and Terrestrial Organic Ice-Nucleating Particles in Pristine Marine to Continentally Influenced Northeast Atlantic Air Masses, *J. Geophys. Res: Atmos.*, 123, 6196-6212, <https://doi.org/10.1029/2017jd028033>, 2018a.
- McCluskey, C. S., Hill, T. C. J., Malfatti, F., Sultana, C. M., Lee, C., Santander, M. V., Beall, C. M., Moore, K. A., Cornwell, G. C., Collins, D. B., Prather, K. A., Jayarathne, T., Stone, E. A., Azam, F., Kreidenweis, S. M., and DeMott, P. J.: A Dynamic Link between Ice Nucleating Particles Released in Nascent Sea Spray Aerosol and Oceanic Biological Activity during Two Mesocosm Experiments, *J. Atmos. Sci.*, 74, 151-166, <https://doi.org/10.1175/Jas-D-16-0087.1>, 2017.
- McCluskey, C. S., Hill, T. C. J., Humphries, R. S., Rauker, A. M., Moreau, S., Stratton, P. G., Chambers, S. D., Williams, A. G., McRobert, I., Ward, J., Keywood, M. D., Harnwell, J., Ponsonby, W., Loh, Z. M., Krummel, P. B., Protat, A., Kreidenweis, S. M., and DeMott, P. J.: Observations of Ice Nucleating Particles Over Southern Ocean Waters, *Geophys. Res. Lett.*, 45, <https://doi.org/10.1029/2018gl079981>, 2018b.
- Meng, X., Yu, Y., and Ginoux, P.: Rise in dust emissions from burned landscapes primarily driven by small fires, *Nat. Geosci.*, 18, 586-592, <https://doi.org/10.1038/s41561-025-01730-3>, 2025.
- Meyers, M. P., DeMott, P. J., and Cotton, W. R.: New primary ice-nucleation parameterizations in an explicit cloud model, *J. Appl. Meteor. Climatol.*, 31, 708-721, 1992.
- Miltenberger, A. K., Field, P. R., Hill, A. A., Rosenberg, P., Shipway, B. J., Wilkinson, J. M., Scovell, R., and Blyth, A. M.: Aerosol–cloud interactions in mixed-phase convective clouds–Part 1: Aerosol perturbations, *Atmos. Chem. Phys.*, 18, 3119-3145, 2018.
- Murray, B. J., O'Sullivan, D., Atkinson, J. D., and Webb, M. E.: Ice nucleation by particles immersed in supercooled cloud droplets, *Chem Soc Rev*, 41, 6519-6554, <https://doi.org/10.1039/c2cs35200a>, 2012.
- Niemand, M., Möhler, O., Vogel, B., Vogel, H., Hoose, C., Connolly, P., Klein, H., Bingemer, H., DeMott, P., Skrotzki, J., and Leisner, T.: A Particle-Surface-Area-Based Parameterization of Immersion Freezing on Desert Dust Particles, *J. Atmos. Sci.*, 69, 3077-3092, <https://doi.org/10.1175/Jas-D-11-0249.1>, 2012.
- Norris, G., Duvall, R., Brown, S., and Bai, S.: EPA positive matrix factorization (PMF) 5.0 fundamentals and user guide, US Environmental Protection Agency, Washington, DC, [www2.epa.gov/sites/production/files/2015-02/documents/pmf\\_5.0\\_user\\_guide.pdf](http://www2.epa.gov/sites/production/files/2015-02/documents/pmf_5.0_user_guide.pdf), 2014.



- 945 O'Sullivan, D., Murray, B. J., Ross, J. F., and Webb, M. E.: The adsorption of fungal ice-nucleating proteins on mineral dusts: a terrestrial reservoir of atmospheric ice-nucleating particles, *Atmos. Chem. Phys.*, 16, 7879-7887, <https://doi.org/10.5194/acp-16-7879-2016>, 2016.
- O'Sullivan, D., Murray, B. J., Malkin, T. L., Whale, T. F., Umo, N. S., Atkinson, J. D., Price, H. C., Baustian, K. J., Browse, J., and Webb, M. E.: Ice nucleation by fertile soil dusts: relative
- 950 importance of mineral and biogenic components, *Atmos. Chem. Phys.*, 14, 1853-1867, <https://doi.org/10.5194/acp-14-1853-2014>, 2014.
- Pereira, D. L., Gavián, I., Letechipía, C., Raga, G. B., Puig, T. P., Mugica-Álvarez, V., Alvarez-Ospina, H., Rosas, I., Martinez, L., Salinas, E., Quintana, E. T., Rosas, D., and Ladino, L. A.: Mexican agricultural soil dust as a source of ice nucleating particles, *Atmos. Chem. Phys.*, 22,
- 955 6435-6447, <https://doi.org/10.5194/acp-22-6435-2022>, 2022.
- Pratt, K. A., DeMott, P. J., French, J. R., Wang, Z., Westphal, D. L., Heymsfield, A. J., Twohy, C. H., Prenni, A. J., and Prather, K. A.: In situ detection of biological particles in cloud ice-crystals, *Nat. Geosci.*, 2, 398-401, <https://doi.org/10.1038/ngo521>, 2009.
- Pratt, K. A., Twohy, C. H., Murphy, S. M., Moffet, R. C., Heymsfield, A. J., Gaston, C. J.,
- 960 DeMott, P. J., Field, P. R., Henn, T. R., Rogers, D. C., Gilles, M. K., Seinfeld, J. H., and Prather, K. A.: Observation of playa salts as nuclei in orographic wave clouds, *J. Geophys. Res: Atmos.*, 115, <https://doi.org/10.1029/2009jd013606>, 2010.
- Prenni, A. J., DeMott, P. J., Sullivan, A. P., Sullivan, R. C., Kreidenweis, S. M., and Rogers, D. C.: Biomass burning as a potential source for atmospheric ice nuclei: Western wildfires and prescribed burns, *Geophys. Res. Lett.*, 39, <https://doi.org/10.1029/2012gl051915>, 2012.
- 965 Reicher, N., Budke, C., Eickhoff, L., Raveh-Rubin, S., Kaplan-Ashiri, I., Koop, T., and Rudich, Y.: Size-dependent ice nucleation by airborne particles during dust events in the eastern Mediterranean, *Atmos. Chem. Phys.*, 19, 11143-11158, 2019.
- Rolph, G., Stein, A., and Stunder, B.: Real-time environmental applications and display system: READY, *Environ. Model. Softw.*, 95, 210-228, 2017.
- 970 Schill, G. P., DeMott, P. J., Emerson, E. W., Rauker, A. M. C., Kodros, J. K., Suski, K. J., Hill, T. C. J., Levin, E. J. T., Pierce, J. R., Farmer, D. K., and Kreidenweis, S. M.: The contribution of black carbon to global ice nucleating particle concentrations relevant to mixed-phase clouds, *Proc. Natl. Acad. Sci. USA*, 117, 22705-22711, <https://doi.org/10.1073/pnas.2001674117>, 2020.
- 975 Schnell, R. C. and Vali, G.: Looking Back: An Account of How Ice Nucleation by Bacteria Was Discovered (1963 to about Mid-1980s). Part II: Broadening the Scope, *Bull. Amer. Meteor. Soc.*, 105, E1004-E1014, <https://doi.org/10.1175/bams-d-23-0115.1>, 2024.
- Seinfeld, J. H. and Pandis, S. N.: Atmospheric chemistry and physics: from air pollution to climate change, 3<sup>rd</sup> edn., Wiley, Hoboken, NJ, 2016.
- 980 Seinfeld, J. H., Bretherton, C., Carslaw, K. S., Coe, H., DeMott, P. J., Dunlea, E. J., Feingold, G., Ghan, S., Guenther, A. B., Kahn, R., Kraucunas, I., Kreidenweis, S. M., Molina, M. J., Nenes, A., Penner, J. E., Prather, K. A., Ramanathan, V., Ramaswamy, V., Rasch, P. J., Ravishankara, A. R., Rosenfeld, D., Stephens, G., and Wood, R.: Improving our fundamental understanding of the role of aerosol-cloud interactions in the climate system, *Proc. Natl. Acad. Sci. USA*, 113, 5781-
- 985 5790, <https://doi.org/10.1073/pnas.1514043113>, 2016.





- Shawon, A. S. M., Benedict, K. B., Gutierrez, A., and Aiken, A. C.: Diurnal Trends and Meteorological Factors Influencing the Variability of Fluorescent Bioaerosol in Mt. Crested Butte, Colorado During SAIL, *J. Geophys. Res: Atmos.*, 130, <https://doi.org/10.1029/2024jd041186>, 2025.
- 990 Shi, Y., Creamean, J., Hill, T., Hume, C., & Vazquez, M. Ice Nucleation Spectrometer for INP measurement (INP), 2021-09-09 to 2023-06-12, ARM Mobile Facility (GUC), Gunnison, CO; Supplemental Facility 2 (S2). Atmospheric Radiation Measurement (ARM) User Facility. <https://doi.org/10.5439/1770816>, Data accessed 2025-05-01.
- Shi, Y. and Liu, X.: Dust radiative effects on climate by glaciating mixed-phase clouds, *Geophys. Res. Lett.*, 46, 6128-6137, 2019.
- 995 Stein, A. F., Draxler, R. R., Rolph, G. D., Stunder, B. J., Cohen, M. D., and Ngan, F.: NOAA's HYSPLIT atmospheric transport and dispersion modeling system, *Bull. Amer. Meteor. Soc.*, 96, 2059-2077, 2015.
- Steinke, I., Funk, R., Busse, J., Iturri, A., Kirchen, S., Leue, M., Möhler, O., Schwartz, T., Schnaiter, M., Sierau, B., Toprak, E., Ullrich, R., Ulrich, A., Hoose, C., and Leisner, T.: Ice nucleation activity of agricultural soil dust aerosols from Mongolia, Argentina, and Germany, *J. Geophys. Res: Atmos.*, 121, <https://doi.org/10.1002/2016jd025160>, 2016.
- 1000 Storelvmo, T., Hoose, C., and Eriksson, P.: Global modeling of mixed-phase clouds: The albedo and lifetime effects of aerosols, *J. Geophys. Res: Atmos.*, 116, 2011.
- 1005 Sun, Y., Zhu, Y., Qi, Y., Chen, L., Mu, J., Shan, Y., Yang, Y., Nie, Y., Liu, P., Cui, C., Zhang, J., Liu, M., Zhang, L., Wang, Y., Wang, X., Tang, M., Wang, W., and Xue, L.: Measurement report: Atmospheric ice nuclei in the Changbai Mountains (2623 m a.s.l.) in northeastern Asia, *Atmos. Chem. Phys.*, 24, 3241-3256, <https://doi.org/10.5194/acp-24-3241-2024>, 2024.
- Suski, K. J., Hill, T. C., Levin, E. J., Miller, A., DeMott, P. J., and Kreidenweis, S. M.: Agricultural harvesting emissions of ice-nucleating particles, *Atmos. Chem. Phys.*, 18, 13755-13771, 2018.
- 1010 Testa, B., Hill, T. C. J., Marsden, N. A., Barry, K. R., Hume, C. C., Bian, Q., Uetake, J., Hare, H., Perkins, R. J., Möhler, O., Kreidenweis, S. M., and DeMott, P. J.: Ice Nucleating Particle Connections to Regional Argentinian Land Surface Emissions and Weather During the Cloud, Aerosol, and Complex Terrain Interactions Experiment, *J. Geophys. Res: Atmos.*, 126, <https://doi.org/10.1029/2021jd035186>, 2021.
- Tobo, Y., DeMott, P. J., Hill, T. C. J., Prenni, A. J., Swoboda-Colberg, N. G., Franc, G. D., and Kreidenweis, S. M.: Organic matter matters for ice nuclei of agricultural soil origin, *Atmos. Chem. Phys.*, 14, 8521-8531, <https://doi.org/10.5194/acp-14-8521-2014>, 2014.
- 1020 Tobo, Y., Prenni, A. J., DeMott, P. J., Huffman, J. A., McCluskey, C. S., Tian, G., Pöhlker, C., Pöschl, U., and Kreidenweis, S. M.: Biological aerosol particles as a key determinant of ice nuclei populations in a forest ecosystem, *J. Geophys. Res: Atmos.*, 118, <https://doi.org/10.1002/jgrd.50801>, 2013.
- Umo, N. S., Murray, B. J., Baeza-Romero, M. T., Jones, J. M., Lea-Langton, A. R., Malkin, T. L., O'Sullivan, D., Neve, L., Plane, J. M. C., and Williams, A.: Ice nucleation by combustion ash particles at conditions relevant to mixed-phase clouds, *Atmos. Chem. Phys.*, 15, 5195-5210, <https://doi.org/10.5194/acp-15-5195-2015>, 2015.
- 1025



- Vali, G.: Quantitative evaluation of experimental results on the heterogeneous freezing nucleation of supercooled liquids, *J. Atmos. Sci.*, 28, 402-409, 1971.
- 1030 Vali, G. and Schnell, R. C.: Looking Back: An Account of How Ice Nucleation by Bacteria Was Discovered (1963 to about Mid-1980s). Part I: The Basics, *Bull. Amer. Meteor. Soc.*, 105, E778-E788, <https://doi.org/10.1175/bams-d-23-0114.1>, 2024.
- Viviroli, D., Dürr, H. H., Messerli, B., Meybeck, M., and Weingartner, R.: Mountains of the world, water towers for humanity: Typology, mapping, and global significance, *Water Resour. Res.*, 43, 2007.
- 1035 Wagner, R., Jähn, M., and Schepanski, K.: Wildfires as a source of airborne mineral dust—revisiting a conceptual model using large-eddy simulation (LES), *Atmos. Chem. Phys.*, 18, 11863-11884, 2018.
- Wilson, T. W., Ladino, L. A., Alpert, P. A., Breckels, M. N., Brooks, I. M., Browse, J., Burrows, S. M., Carslaw, K. S., Huffman, J. A., Judd, C., Kilhau, W. P., Mason, R. H., McFiggans, G., Miller, L. A., Najera, J. J., Polishchuk, E., Rae, S., Schiller, C. L., Si, M., Temprado, J. V., Whale, T. F., Wong, J. P., Wurl, O., Yakobi-Hancock, J. D., Abbatt, J. P., Aller, J. Y., Bertram, A. K., Knopf, D. A., and Murray, B. J.: A marine biogenic source of atmospheric ice-nucleating particles, *Nature*, 525, 234-238, <https://doi.org/10.1038/nature14986>, 2015.
- 1040 Zhao, X., Jiang, K., Ou'yang, S., Li, Y., Wang, Y., Wang, J., Zhao, N., and Shen, G.: Global Biomass Burning Emission Contributions to Ice Nucleating Particles, *Geophys. Res. Lett.*, 51, <https://doi.org/10.1029/2024gl111881>, 2024.
- Ruichen Zhou, Russell Perkins, Sonia Kreidenweis. Source apportionment of aerosols at the White River IMPROVE site near the SAIL site. ARM Data Collection, Oak Ridge National Laboratory, U.S. Department of Energy, Oak Ridge, Tennessee, USA. Dataset accessed on 2025. <https://doi.org/10.5439/2573028>, 2025a.
- 1050 Ruichen Zhou, Russell Perkins, Sonia Kreidenweis, Kelton Ayars. Back trajectories during SAIL. ARM Data Collection, Oak Ridge National Laboratory, U.S. Department of Energy, Oak Ridge, Tennessee, USA. Dataset accessed on 2025. <https://doi.org/10.5439/2574969>, 2025a.
- 1055 Ruichen Zhou, Russell Perkins, Sonia Kreidenweis. Merged aerosol size distribution from SMPS and OPC for SAIL. ARM Data Collection, Oak Ridge National Laboratory, U.S. Department of Energy, Oak Ridge, Tennessee, USA. Dataset accessed on 2025. <https://doi.org/10.5439/2572899>, 2025a.